View metadata, citation and similar papers at core.ac.uk

brought to you by CORE

provided by Illinois Digital Environment for Access to Learning and Scholarship Repository

WMRC Reports

Waste Management and Research Center

Metal Distribution and Speciation at the DePue Wildlife Management Area

Paul Anderson
Grant Bunker
Shinwoo Lee
Firouzeh Tannazi

Illinois Institute of Technology

RR-99
November 2002
Printed on Recycled Paper

$5

This report is part of WMRC's Research Report Series. Mention of trade names or commercial products does not constitute endorsement or recommendation for use.

About WMRC's Electronic Publications:

This document was originally published in a traditional format.

It has been transferred to an electronic format to allow faster and broader access to important information and data.

While the Center makes every effort to maintain a level of quality during the transfer from print to digital format, it is possible that minor formatting and typographical inconsistencies will still exist in this document.

Additionally, due to the constraints of the electronic format chosen, page numbering will vary slightly from the original document.

The original, printed version of this document may still be available.

Please contact WMRC for more information:

WMRC
One E. Hazelwood Drive
Champaign, IL 61820
217-333-8940 (phone)

www.wmrc.uiuc.edu

WMRC is a division of the Illinois Department of Natural Resources

RR-99

Metal Distribution and Speciation at the DePue Wildlife Management Area

Paul Anderson
Grant Bunker
Shinwoo Lee
Firouzeh Tannazi

Illinois Institute of Technology

November 2002

Submitted to:

Illinois Waste Management and Research Center
1 E. Hazelwood Dr.
Champaign, IL 61820
www.wmrc.uiuc.edu

Printed by the Authority of the State of Illinois
2002/50

Acknowledgments

A danger with acknowledgments is that someone who belongs here will be left out. Anyway; here goes. There are many people who are or were associated with the Illinois Waste Management and Research Center who played a role in the success of this project. That group includes M. Piwoni, J. Talbott, J. Hafermann, S. Davis, R. Farrell, T. Chow, and M. Wilcoxon. Investigators and workers on the other projects at the DWMA were either in the field and/or sharing ideas about what we all found. A special thanks to T. Holm who originally suggested the idea that metal sorption to oxides could play an important role at the DWMA. Other members of that group include A. Wehrmann, J. Levengood, K. Carr, R., Cahill, and W. Kelly. We all needed other ILEPA and ILDNR personnel to make the project work, especially R. Lange and M. Resetich. A. Atkins was a tremendous resource for help with ArcView. Finally, thanks to the staff and volunteer students who helped with measurements at BioCAT and MRCAT. Use of the Advanced Photon Source was supported by the U. S. Department of Energy, Basic Energy Sciences, Office of Science, under Contract No. W-31-109-Eng-38.

Table of Contents

List of Tables

List of Figures

Abstract

The objective of this study was to assess the distribution and speciation of cadmium (Cd), copper (Cu), lead (Pb), and zinc (Zn) in soils of the DePue Wildlife Management Area (DWMA) near DePue, IL. More than 70 soil cores were collected at the site. These cores were subdivided and soils from several depths were analyzed to determine the total concentration of each metal in the soil. The sample scheme was developed so that the data would also be useful in a geostatistical assessment of the site. A subset of 14 cores was used to assess metal speciation based on an extraction process. Metal speciation in these same cores was also assessed using x-ray absorption spectroscopy (XAS).

Mean concentrations from samples of each metal throughout the site were Cd = 45, Cu = 95, Pb = 210, and Zn = 2772 mg/kg. Speciation results suggest that Cd and Zn, which are substantially associated with exchangeable, iron (Fe) and manganese (Mn) oxide, and carbonate fractions of the soil, probably exhibit the greatest mobility. In contrast, Pb and especially Cu are probably much less mobile because they have greater association with organic and residual phases of the soil. Changes in concentration with depth in the soil indicate that Cd and Zn and to a lesser extent Pb are enriched in the upper layers. The horizontal distribution of metals reveals a zone of higher concentration near the center of the northern boundary of the DWMA.

The results are consistent with a conceptual model that describes how the flow of groundwater into and out of the DWMA determines metal mobility. Groundwater seeping into the site first mobilizes and then transports metals upward through the soil column. Metals that are transported to the surface can react with newly precipitated Fe & Mn oxides. As a result, within a soil column the upper soil layers become relatively enriched with metals. Looking across the horizontal surface of the DWMA, the lower elevations are exposed to more frequent flooding and metal concentrations in those areas tend to be higher.

Mobilized metals that are not transported all the way to the surface are transported away from the DWMA with retreating groundwater levels. Relative to the groundwater velocity, however, metal transport is slower because of interactions with clay mineral surfaces. The mobility of the metals probably follows the sequence: Cd > Zn > Pb > Cu.

Both the data and conceptual model developed from this study should be applied to a comprehensive risk assessment for the DWMA. Our results suggest where additional data are needed, likely exposure pathways, and which metals pose relatively greater risks. Subsequent work and any potential remediation activities at the site can benefit from the geostatistical techniques applied here.

XAS analyses can provide important speciation information for remediation work. Unfortunately, the XAS analyses in this study were problematic and largely unsuccessful. Some of the difficulties were related to short-term issues, specific to the timing of this project. Other problems were of a longer-term nature and more generic to XAS applications in environmental research. Experience gained from this project helped suggest solutions to these longer-term problems. New technologies, including the Multilayer Array Analyzer Detector, the Bent Laue Analyzer, and resonant x-ray inelastic scattering are briefly discussed.

Chapter 1. Overview and Introduction

Located approximately one mile south of the city of DePue in Bureau County, Illinois, the DePue Wildlife Management Area (DWMA) rests on a peninsula between Lake DePue and the Illinois River. The site was constructed in 1982 when about 449,000 cubic yards of sediment were dredged and pumped from Lake DePue. Earthen dikes surround the site, which rises about eight feet above the surrounding fields. Illinois Department of Natural Resources personnel believe the sediment within the DWMA is three to four feet deep.

The DWMA (Figure 1) includes a long rectangular section that stretches 3430-ft from east to west and 1090-ft north-to-south. A smaller rectangular section juts out 730-ft to the north for 800-ft along the east end of the northern boundary. Boundaries for the DWMA are very regular except where notches are cut out in the extreme northeast corner and near the middle of the northern boundary. A primitive road tops the perimeter dike around the site. An irregular, intermittent road also tops a dike that meanders across the site, effectively dividing the DWMA into three large zones and one small zone.

Within these zones the surface topography is relatively flat, with an average elevation just under 450 ft above sea level. A contour map prepared from data collected in this study (Figure 2) suggests that low points are in the northeast corners and through the center of the site. This map, however, is based on a relatively small data set and should be used cautiously. Furthermore, the map does not take into account the dikes and roads that run through the site.

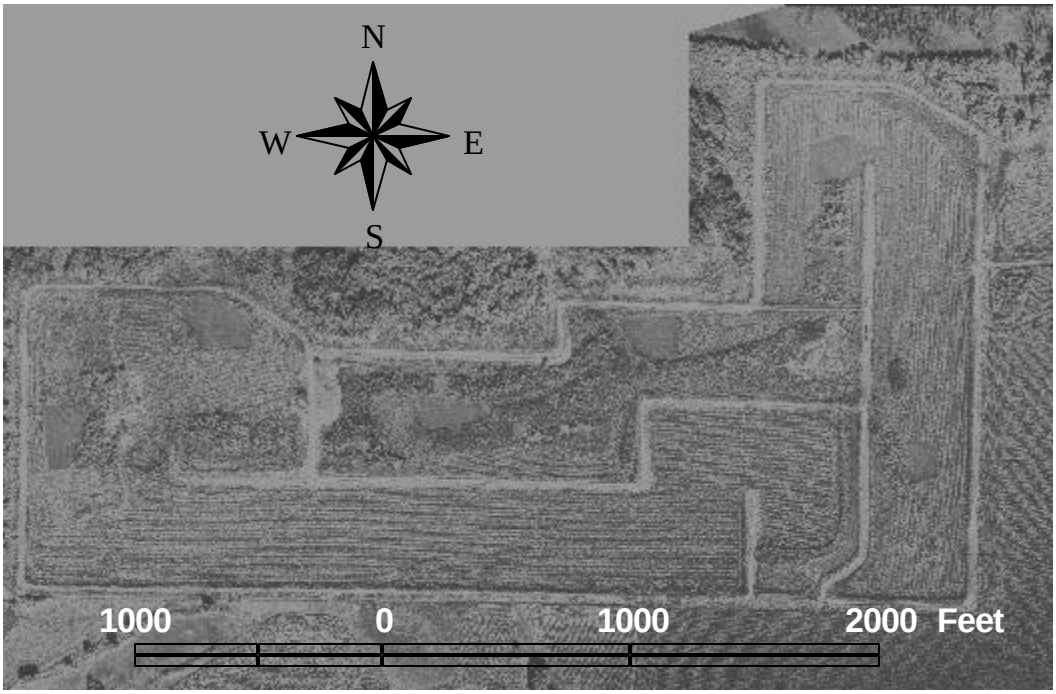

Figure 1. Aerial view of the DWMA.

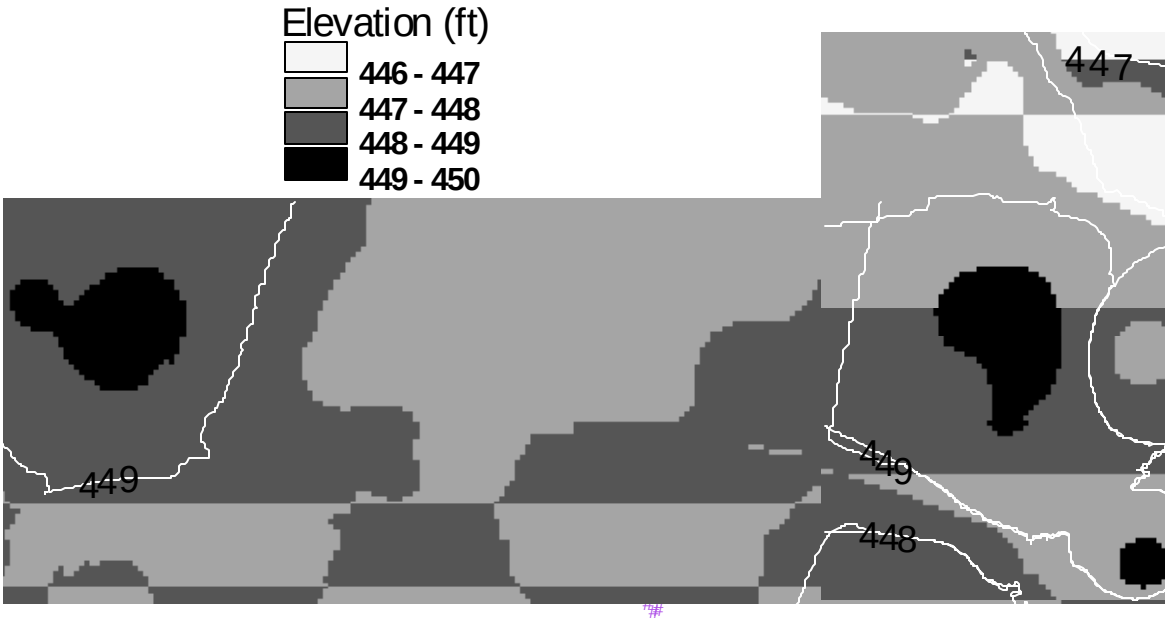

Figure 2. Contour map of interpolated surface elevation (ft above sea level) at the DWMA.

The work described here was part of a multi-disciplinary, comprehensive study on potential environmental effects of metals in the soil at the DWMA. This portion of the study deals specifically

with metal speciation and distribution at the site. It is important to recognize that the data described here come from an initial survey of the site. The original plan was to use data from this study to design a more detailed survey that would better capture the spatial resolution of metals in the soil. In the absence of that additional information, the reader should be aware that interpolation results presented here are based on limited data. Rather than presenting a comprehensive description of metal distribution at the site, these results indicate where additional data are needed and demonstrate how the interpolation tools can be used to guide remediation decisions.

This report begins with a review of methodology, including sample collection, processing and analyses, and data evaluation. Results presented in the next section describe conventional statistics of these measurements, the spatial variability of the data, and the species of metals that exist at the site. This information is integrated in the discussion and conclusion sections. The report concludes with recommendations, a list of references cited in the text, and supporting information in the appendices.

Chapter 2. Methodology

Introduction

This chapter includes brief descriptions of the methods used in this project, from collecting soil cores in the field, through sample processing and analysis, to evaluation of the data. In many cases, the brief descriptions provided here also contain citations where much more detailed discussions of the analytical methods can be found.

Sample Locations

The overall objective of the sample plan was to collect representative soil samples from the DWMA that could be used to explore metal speciation and efficiently estimate the unknown spatial scale of variation for concentrations of metals at the site. A nested sample scheme was used with five samples collected from each of 14 cells at the site. (Cells and sample locations can be seen in Figure 3. Because of the scale in this figure, the closest sample locations appear as one symbol.)

The site was divided into 14 cells to ensure that samples came from throughout the DWMA. Specific sample locations for the five samples within each cell were randomly selected, but the distances between samples were pre-selected to provide information on the spatial continuity. The rationale for this sampling scheme is discussed below in the section on geostatistical analysis.

Sample locations were flagged and identified using global positioning system (GPS) surveying. Raw data from these measurements and a brief description of the GPS process are in a report by Locke (1998), which is included in Appendix A.

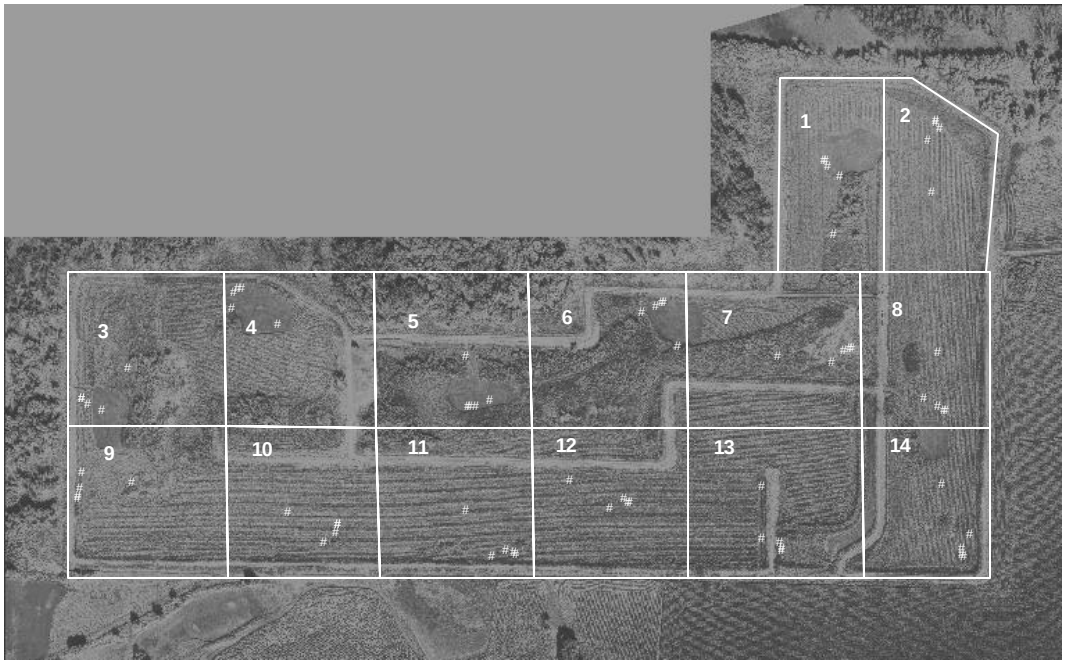

Figure 3. Cells and soil sample locations at the DePue Wildlife Management Area.

Sample Collection

Soil cores were collected by hand or, when access by road was convenient, by a truck-mounted Geoprobe (a mobile, well-drilling device). In either case, a plastic liner (1.5-in diameter, 4-ft long) was inserted into a stainless steel tube (2-in outer diameter, 1.5-in inner diameter, slightly more than 4-ft long). The tube was driven into the soil (by hand or the Geoprobe anvil) to a depth of about 4-ft. The tube was recovered (using a hand-operated lever or reversing the Geoprobe), the liner was removed, and both ends were covered with vinyl caps. These sample cores were sawed in half. The newly exposed ends were also covered with vinyl caps and the now 2-ft cores were stored in a cooler. Most of these samples were transported to the Illinois Waste Management and Research Center (WMRC) and stored under refrigeration until further processing for analyses to determine soil carbon and total metals concentrations. A subset of 14 cores was transported to the Illinois Institute of Technology and stored under refrigeration until processing for metal speciation studies.

Sample Processing and Analyses for Metals and Carbon

A detailed description of the sample processing and analyses is in the report by Talbott and Piwoni (1998), which is included in Appendix B. Briefly, cores were sectioned into approximately 1-ft (30-cm) intervals. Representative subsamples (≈ 30-g) were weighed, dried, weighed again to determine moisture content, ground to < 10-μm diameter, transferred to polypropylene bottles, and stored in a desiccator prior to digestion. The powders were subjected to microwave acid-digestion and filtration (Whatman #40) to

remove residual solids. Total metal (Cd, Cu, Pb, and Zn) concentrations in the filtrates were determined by Inductively Coupled Plasma Mass Spectrometry (ICP-MS) at the WMRC.

In addition, a subset (random) of the cores was analyzed (also at the WMRC) to determine total carbon (TC), total inorganic carbon (TIC), and total organic carbon (TOC) by difference. These analyses were made using a UIC Coulometric carbon analyzer at the WMRC.

Extractions

A subset (random) of ten sample cores was evaluated. Two of these cores were duplicate cores collected in the field. Two of the remaining eight cores were processed in duplicate. In each case, a 10-g sample of soil was removed from the top 2-in (5-cm) of the soil core. (Only the top 2-in were used because in our original plan, x-ray absorption spectroscopy (XAS) would be used to assess metal speciation throughout the column. These extractions were supposed to merely confirm the XAS results.) This sample was air-dried, then crushed, and the material that passed through a 1.18-mm sieve was processed using the sequential extraction procedure described by Tessier et al. (1979). This extraction procedure relies on an operational definition of the soil fraction released by a series of four extractants (Table 1). A fifth step was designed to dissolve the residual mineral phase. Extracts resulting from all five steps were analyzed (ICP-MS) at the WMRC.

Table 1. Operationally defined fraction and associated chemicals used in the extraction. See the article by Tessier et al. (1979) for more details.

Fraction	Extractant
Exchangeable	$MgCl_2$
Carbonate	NaOAc
Fe-Mn Oxide	$NH_2OH.HCl$ + HOAc
Organic Matter	HNO_3 + H_2O_2
Residual	$HClO_4$ + HF + HCl

X-ray Diffraction

Soil samples were air-dried at room temperature, crushed, and the clay fraction was isolated from material that passed through a 425 μm sieve. Clay isolation involved removal of organic matter followed by a series of washing, centrifugation, and re-suspension steps; dispersion; and finally separation by sedimentation. More details on these processing steps are available in the reference by Moore and Reynolds (1997). The final clay suspension was applied to a glass slide and allowed to dry at room temperature prior to the x-ray diffraction measurements.

We obtained reference clay mineral samples from the Source Clay Mineral Repository at the University of Missouri. These samples, used as received without further processing, were sprinkled on glass slides that were coated with a thin layer of petroleum jelly.

X-ray Absorption Spectroscopy

One goal of the study was to compare speciation data from traditional extractions to speciation data obtained from x-ray absorption spectroscopy (XAS). XAS is a powerful analytical tool that can be used to describe the local electronic environment of specific elements. In contrast with the extraction studies traditionally used to describe metal speciation, XAS evaluates conditions from the perspective of the target element. This approach avoids the operational definition of speciation and the redistribution of metals that can occur with extraction techniques. Brown (1990) provides a more detailed description of XAS techniques.

X-ray absorption measurements were carried out on MR-CAT beamline ID-10 and BioCAT beamline ID-18 at the Advanced Photon Source. Liquid nitrogen cooled silicon (111) crystal monochromators were used initially in step-scan mode and later in continuous scan mode. In all cases harmonics were rejected by positioning the harmonic rejection mirror at an appropriate angle. To monitor the incident flux, ionization chambers were used, filled with either nitrogen or helium. The ionization chambers were operated in their plateau region to ensure linearity. Zn concentrations were sufficiently high that conventional Lytle detectors with Cu filter and Soller slits were adequate despite the presence of a large amount of Fe fluorescence from the sample matrix. Standards were purchased from commercial suppliers, or in the case of metals adsorbed to HFO and montmorillonite, they were prepared in our laboratory according to established procedures. The solid standards were ground in a mortar and pestle, sieved to 400 mesh (<38 micrometer), and applied to adhesive film, which was checked for an absence of Zn. A single layer of the sample was measured to ensure the samples were in the thin concentrated limit and the measured spectra accurately reflected the true spectra.

To perform the measurements in the least intrusive manner, initial measurements were made by placing the whole core into the x-ray beam. A slot was milled in the plastic tube containing each core, and the opening was covered with a 2 mil mylar window through which the incident x-ray beam could enter and the x-ray fluorescence could escape. We then measured the x-ray absorption spectrum as a function of depth (position along the length of the core). Unfortunately, the surface topography caused systematic modulations in the edge step at different positions along the sample. Subsequent measurements were made by first removing a soil sample from a specific position along the core and placing that sample in a holder positioned in the beam. All results presented in this report were obtained in this way.

Standard methods of data reduction were carried out using the University of Washington XAFS programs and programs written in-house in Mathematica. Specifically the steps are: data deglitching, averaging, normalization, interpolation to k-space, and background subtraction with cubic splines.

Several methods of fitting the data were explored in the programming environment Mathematica: Linear least squares fitting without constraints; singular value decomposition without constraints; nonlinear least squares fitting constrained to positive values; principal components analysis; and a novel application of linear programming (LP). The most direct and robust approach was the LP method.

Statistical Analyses

Conventional statistical analyses of the data were accomplished using Excel. In addition to considering all the samples, analytical results were subdivided into four subsets, representing average soil depths of about 6-in (0 – 30-cm depth), 18-in (30 – 60-cm depth), 30-in (60 – 90-cm depth), and 39-in (99-cm).

Geostatistical Analyses

Geostatistics is the term used for a family of deterministic and statistical tools used to describe spatial variability. Results presented here, which are based on limited data from a preliminary survey, demonstrate where additional samples are needed and how geostatistics can be used to support remediation decisions. One objective of this study was to look at the spatial distribution of metals at average soil depths of 6-, 18-, and 30-in. Our analysis did not consider the effects of the internal dikes or roads, which could have an effect on metal transport in the DWMA. The first stage of spatial analysis relied on qualitative contour diagrams to examine trends in the data. These diagrams were prepared using inverse distance interpolation, a standard contouring scheme in ArcView. Contour diagrams presented in this study used a power of two and considered the six nearest neighbors.

The second stage of the analyses relied on Geostatistical Environmental Assessment Software (GEO-EAS), public domain software available through the United States Environmental Protection Agency. Basic information about the software is available in the user's guide written by Englund and Sparks (1991). Goals of this stage were to prepare a more quantitative description of spatial continuity for metals at the site and to try to assess the estimation error.

The most common descriptor of spatial continuity in geostatistics is probably the variogram (Isaaks and Srivastava, 1989). The variogram is half the average squared difference between paired values at approximately the same separation distance. (The term "semivariogram", which is sometimes used interchangeably with variogram, is technically correct because a factor of 2 appears in the denominator.)

$$g(h) = \frac{1}{2N(h)} \sum_{(i,j)|h_{ij} \approx h} \left(C_i - C_j\right)^2$$

In this expression, $\gamma(h)$ is the value of the variogram at the distance h, N(h) is the number of paired values that are approximately a distance h apart, and C_i and C_j are the concentration values. The separation distance, h, is called the lag distance. Together, all the separation distances used to define the spatial continuity are called "lags".

In this study, the sample plan was designed with the concept of lags in mind. Design lag distances for the five samples in each cell were 6.6, 26.2, 62.3, and 190-ft (2, 8, 19, and 58-m). In the field, sample sites were located using a tape measure. According to the GPS data, the actual average separation distances were 6.8, 25.6, 62.4, and 194.9-ft.

When pairs of measurements are used to calculate the variogram, some tolerance is allowed in the lag distances. Each lag is defined to include all distances longer than the previous lag distance and shorter than the subsequent lag distance. By inspection of the data, the lag distances used in the GEO-EAS program that resulted in four distinct sets of data were 8, 36, 96, and 210-ft. Theoretically the number of sample pairs we would expect to see at each of these distances is 14, 28, 42, and 56, respectively. For example, there would be 14 sample pairs separated by less than 8-ft, 28 sample pairs separated by less than 36-ft (14 sample pairs separated by about 25.6-ft and another 14 sample pairs separated by 6.8 + 25.6 = 32.4-ft), and so on. In practice, the number of sample pairs was smaller because cores were not retrieved from all sample locations or the length of the core was not adequate. One sample was excluded because the GPS location was inaccurate. Because of the iterative nature of this analysis, more details on the methodology are presented along with the results.

The advantage of this sampling design is that even though relatively few samples were collected, the sample separation distances can help define the spatial continuity. The disadvantage of this approach is that the irregular lag distances can obscure details of the spatial structure.

Quality Assurance and Quality Control

Details of the quality assurance plan for this study can be found in the "Quality Assurance Project Plan for the DePue Wildlife Management Area" (ILDNR, 2001). This section includes a brief description of expected precision for the reported metals concentrations and the expected tolerance for locating the sample positions.

Data for this study provide three different perspectives on precision of the sample collection, handling, and analyses. One perspective is based on measurement of standards and is therefore limited to the

precision of the instrument itself. Acceptance criteria for analyses of independent check standards were ± 10% (Talbott and Piwoni, 1998).

Additional data are available to expand the evaluation of precision to include both instrument analysis and sample processing for digestion. As noted previously, all of the samples were processed using microwave acid digestion prior to analyses. A subset of ten samples was also analyzed for total metal concentrations during the extraction tests for metal speciation. Extracts from both procedures were analyzed using ICP-MS. A scatterplot comparing the two methods (Figure 4) shows good agreement and relatively little consistent bias in the low to middle concentration ranges. (The solid line in the figure represents perfect agreement between the two values.) At the higher concentrations, however, the microwave acid digestion process consistently yielded lower total metal concentrations.

These results can be quantified by estimating the precision associated with the two measurements. Considering each pair of measurements as duplicates and following the procedures outlined in Standard Methods (APHA, 1995), we calculated for each metal the mean of all the duplicates, the standard deviation based on those duplicates, and a coefficient of variation (Table 2). These results suggest a precision ranging from 15% to 22% for the combined operations of digestion and sample processing for analyses.

For carbon analyses, precision based on duplicate measurements did not exceed 3.0%. Accuracy as determined by recovery of a standard ranged from 98% to 102%.

Finally, the most comprehensive assessment of precision of the measurements comes from processing replicate field samples. Duplicate cores were collected adjacent to each other in cells 3, 4, 5, 6, 8, 10, and 13. All cores were processed following identical procedures; after subdividing the cores there were 24 duplicate measurements for each metal. A scatterplot for these measurements (Figure 5) shows relatively good agreement and no consistent bias. There may, however, be a few outliers in the data set, particularly for the highest concentrations. The same approach described above (APHA, 1995) was used to quantify the precision of these data and the results are shown in Table 3. The last row of the table is an indication of the relative precision, expressed as the ratio of standard deviation to the mean. These results suggest the overall precision of these measurements ranges from 13% to 23%.

In summary, these assessments of precision indicate that the instrument error alone is ± 10% but the error increases to ± 15 to 22% when both extraction and analysis are included. There is no further increase in the error when sampling, extraction, and analysis are all considered. Furthermore, with the possible exception of the highest concentrations, there is no systematic bias in the results.

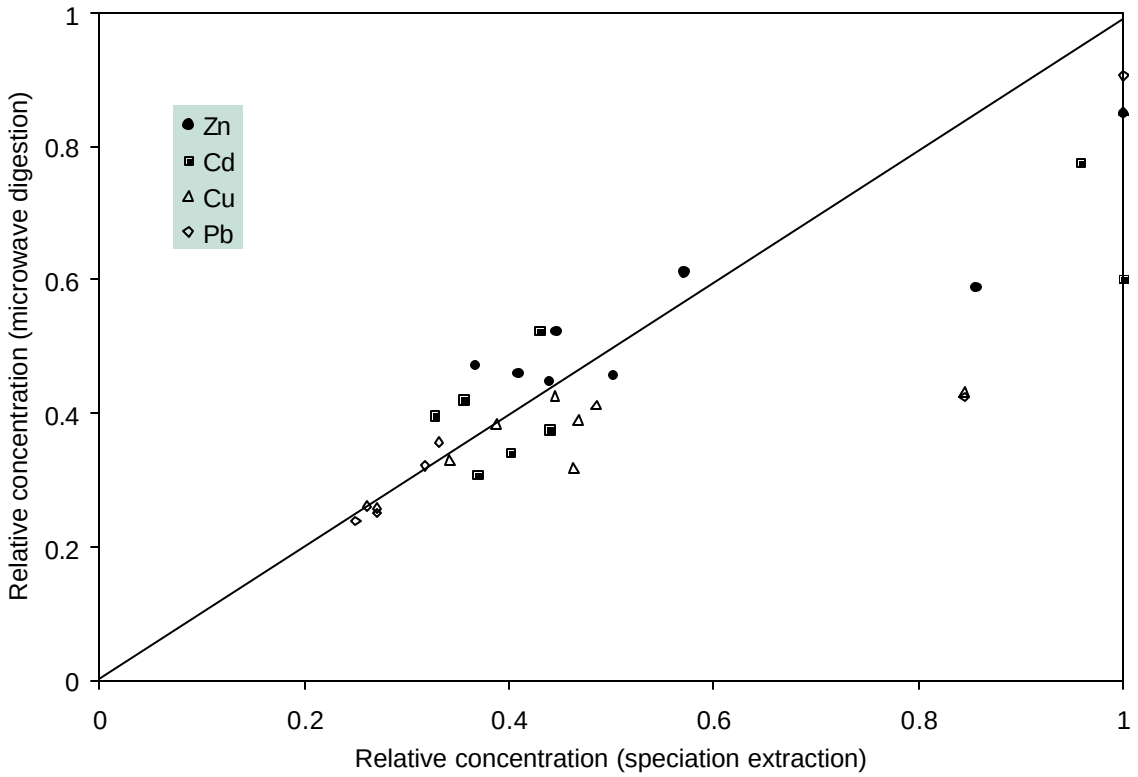

Figure 4. Scatterplot of relative total metal concentrations from two extraction processes. To show all metals on one figure, each concentration is divided by the highest concentration for that metal.

Table 2. Mean, standard deviation, and coefficient of variation for ten samples evaluated using two different extraction processes.

Metal	Cd	Cu	Pb	Zn
Mean (mg/kg)	72.7	132.8	284.6	4436.6
Standard Deviation (mg/kg)	15.9	26.2	45.3	653.1
Coefficient of Variation	0.22	0.20	0.16	0.15

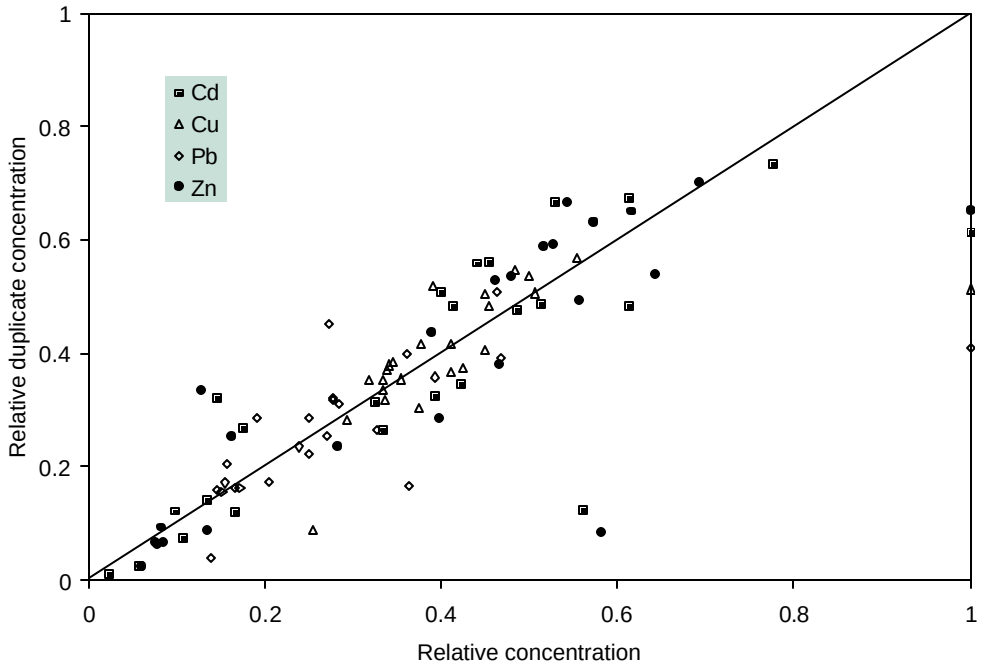

Figure 5. Scatterplot showing relative metal concentrations from duplicate samples. To show all metals on one figure, each concentration is divided by the highest concentration for that metal.

Table 3. Mean, standard deviation, and coefficient of variation for each metal calculated from 24 duplicate measurements.

Metal	Cd	Cu	Pb	Zn
Mean (mg/kg)	42	93	175	2587
Standard Deviation (mg/kg)	9.4	11.9	40.4	549.8
Coefficient of Variation	0.23	0.13	0.23	0.21

Because spatial relationships are important in this study, confidence in the locations of the samples is also important. According to Locke (1998) those measurements should be accurate to +/- 0.07 feet horizontally and +/- 0.13 feet vertically.

Chapter 3. Results

This chapter begins with a statistical description of the data, including minimum, maximum, and median concentration values for each metal at each of three depth intervals. There is also a section on spatial relationships, comparing interpolation results from inverse distance weighting and ordinary block kriging. Finally, the chapter concludes with information on metal speciation within the DWMA and the types of clay minerals that are present.

Conventional Statistical Description of the Data

There were 276 soil samples analyzed for this study. (These data are provided in Appendix C.) The numbers of samples from the 6-, 18-, and 30-in (15-, 45-, and 75-cm) average depth were 67, 64, and 56, respectively. Another 44 samples were in a group that came from 39-in (99-cm) average depth. The remaining 45 samples included 26 replicate samples collected as part of the quality assurance/quality control program, and 19 samples that because of sample loss or sample compression did not fit into any of the above categories. Those 19 samples are not included in this report.

Univariate Description

Univariate statistics for each metal based on all the samples (Table 4) help characterize the distributions. We report three categories of summary statistics here. The mean, median, minimum, and maximum are measures of the location of the distribution. The standard deviation and coefficient of variation measure the spread of the distribution. Finally, kurtosis and skewness measure the shape of the distribution. (The term "distribution" is used here in the sense of standard statistics; it refers to the shape of the histogram or frequency distribution for the data. The spatial distribution of the data is described in an upcoming section.)

The mean and median provide two different measures of the center of the distribution. Because it is the arithmetic average of the data values, the mean can be sensitive to extreme values. In contrast, the median or midpoint of the distribution arranged in increasing value is much less sensitive to high or low values. Because environmental data sets often include extreme values, the median sometimes provides a more appropriate measure of the center of the distribution. In this case, mean and median values for the Cd and Zn distributions are in excellent agreement (±5%). Differences between the mean and median are greater for the Cu and Pb distributions (10% and 17%, respectively), indicating that there are more extreme values in these two distributions. The relative ratio of the mean concentrations is Cd:Cu:Pb:Zn = 1:2.1:4.7:62.

Table 4. Summary univariate statistics for Cd, Cu, Pb, and Zn metal concentrations at the DWMA (n = 276). Dimensions are mg/kg except for coefficient of variation, kurtosis, and skewness, which are dimensionless.

Statistic	Cd	Cu	Pb	Zn
Mean	44.67	95.44	210.40	2772.02
Median	45.95	85.99	173.98	2905.00
Minimum	1.23	9.44	11.95	111.51
Maximum	251.58	769.37	2650.00	15200.00
Standard Deviation	30.39	61.30	232.96	1887.11
Coeff. Variation	0.68	0.64	1.11	0.68
Kurtosis	7.96	61.51	55.58	6.82
Skewness	1.68	6.70	6.58	1.47

Standard deviation values reported in Table 4 measure the spread of the distribution. In this case, where there are several metals and a wide range of means, the coefficient of variation (standard deviation divided by the mean) is a more useful metric. Of the four metals, Pb stands out as the only metal with a coefficient of variation > 1.0, indicating that this distribution has a long tail including some erratic high values.

The last two parameters from Table 4 also provide measures of the shape of the distributions. Kurtosis describes characteristics of the peak of the distribution relative to a normal distribution. With values greater than 0, all four metals have distributions with sharper peaks relative to a normal distribution. Among these metals, Cu and Pb have the sharpest peaks. The skewness describes the degree of symmetry in the distribution. Values greater than 0 indicate a tail in the distribution toward positive values, which is a typical result for environmental data. Once again, Cu and Pb exhibit similar behavior in that the tails of their distributions are larger.

Histograms for the distributions (Figure 6 - Figure 9) provide convenient visual summaries of these statistics. Consistent with data in the table, Cu and Pb have more peaked distributions with longer positive tails; Cd and Zn have flatter distributions.

Variations in Metal Concentrations with Depth

To see how the metal concentrations change with depth, the same summary statistics were calculated for each of the ranges of sample depth. Summarized in Table 5 – Table 8, these values show how the characteristics of the distribution of measured concentrations varied with depth. According to these data the shapes of the distributions change with depth. Decreasing values for the coefficient of kurtosis indicate that the peaks of the distributions are not as sharp and decreasing values of skewness (at least until the 39-in average depth range) suggest the distributions are more normal (extreme high concentrations are not as apparent) at greater depth.

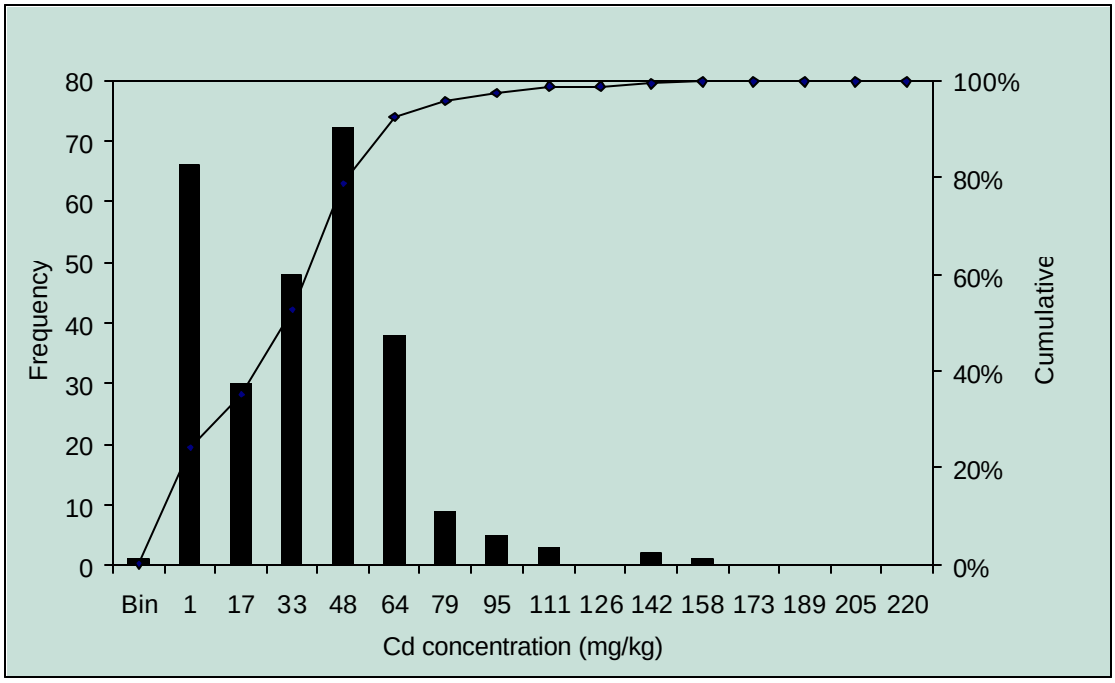

Figure 6. Histogram for Cd based on all sample data from the DWMA.

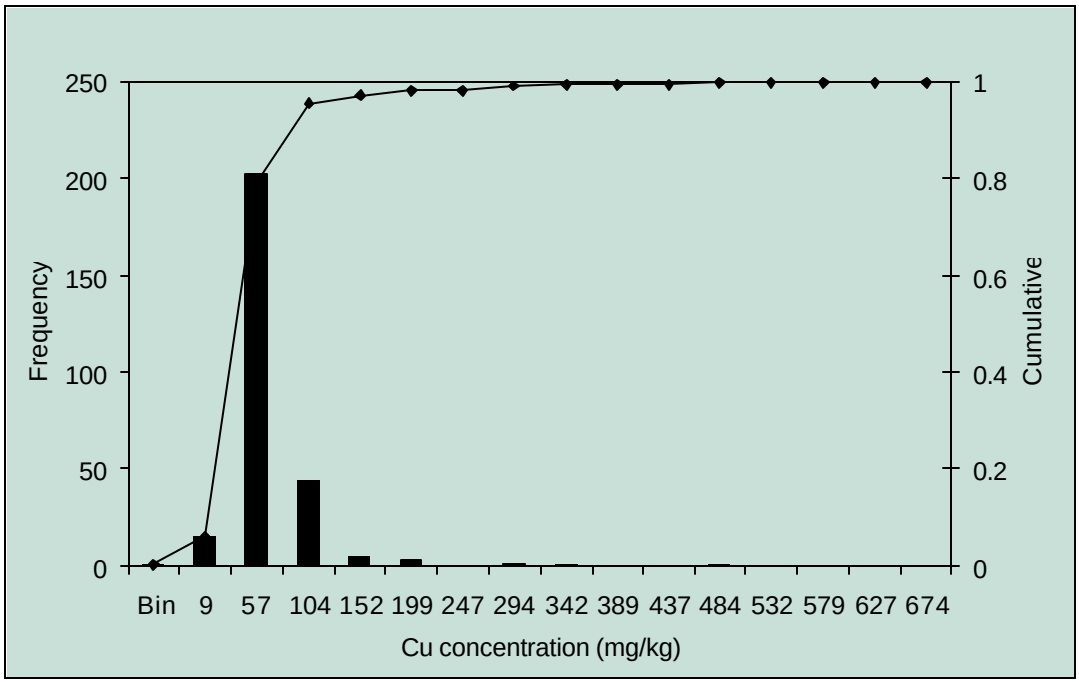

Figure 7. Histogram for Cu based on all sample data from the DWMA.

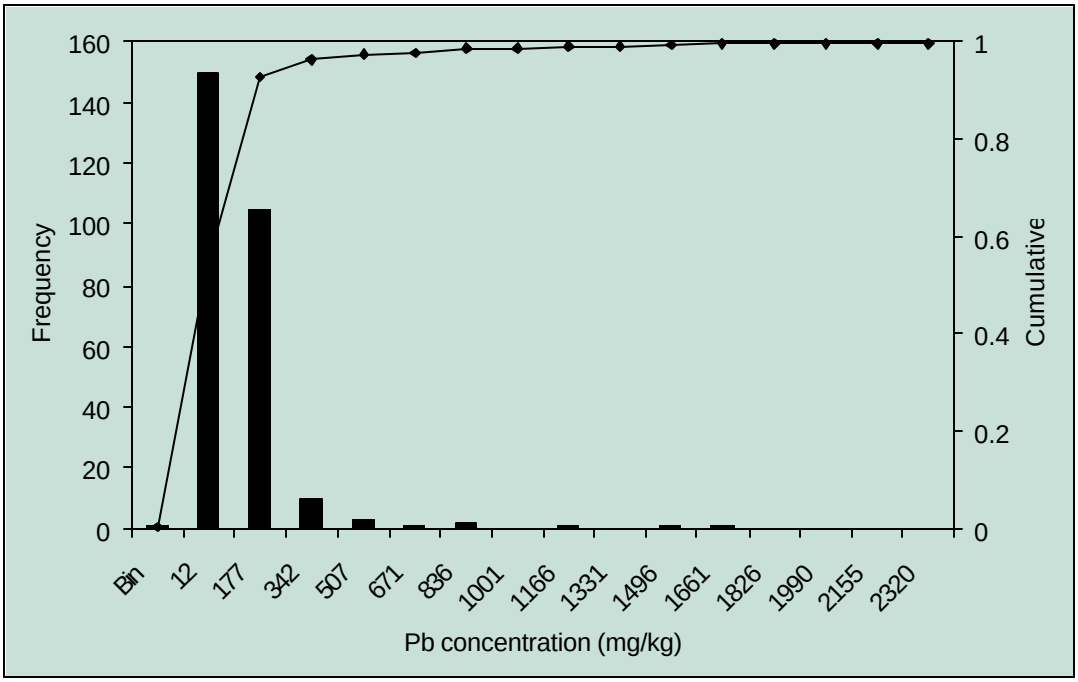

Figure 8. Histogram for Pb based on all sample data from the DWMA.

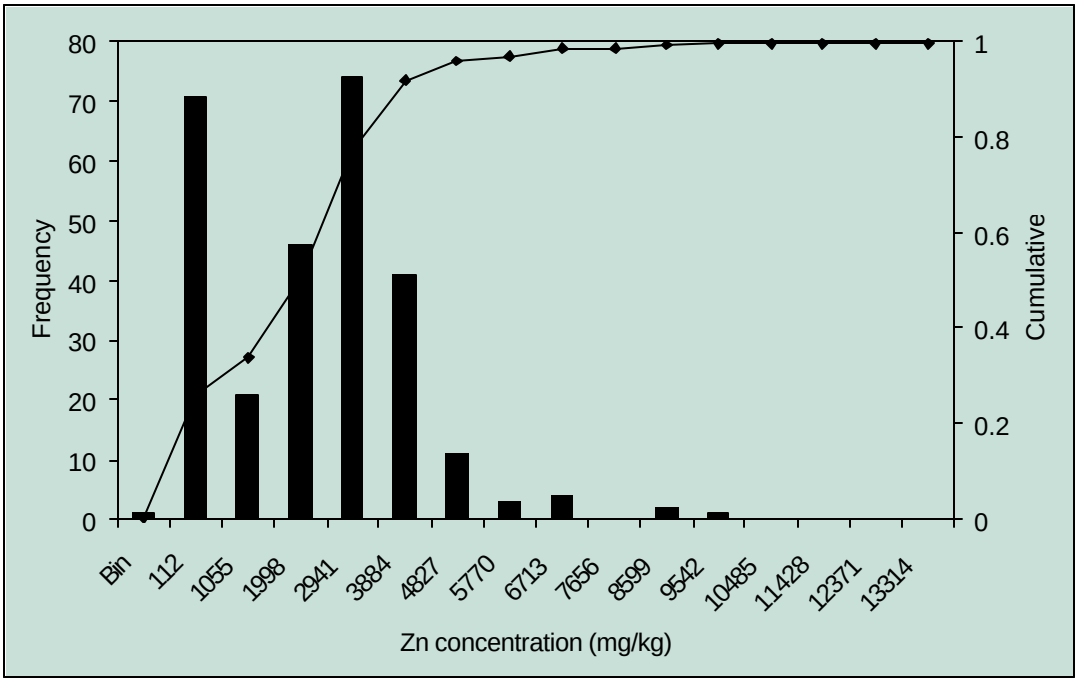

Figure 9. Histogram for Zn based on all sample data from the DWMA.

Table 5. Summary univariate statistics for Cd, Cu, Pb, and Zn metal concentrations at an average depth of 6-in at the DWMA (n = 67). Dimensions are mg/kg except for coefficient of variation, kurtosis, and skewness, which are dimensionless.

Statistic	Cd	Cu	Pb	Zn
Mean	67.27	125.65	325.38	4238.78
Median	59.47	100.74	209.51	3730.00
Minimum	24.91	64.84	124.31	1480.00
Maximum	251.58	769.37	2650.00	15200.00
Standard Deviation	33.88	98.87	378.64	1983.82
Coeff. Variation	0.50	0.79	1.16	0.47
Kurtosis	13.19	28.04	23.09	14.33
Skewness	3.04	4.84	4.44	3.17

Table 6. Summary univariate statistics for Cd, Cu, Pb, and Zn metal concentrations at an average depth of 18-in at the DWMA (n = 64). Dimensions are mg/kg except for coefficient of variation, kurtosis, and skewness, which are dimensionless.

Statistic	Cd	Cu	Pb	Zn
Mean	50.44	93.11	228.77	3075.30
Median	50.50	84.53	180.23	3115.00
Minimum	6.68	9.44	11.95	460.00
Maximum	149.37	493.50	1770.00	8780.05
Standard Deviation	23.12	56.20	221.53	1358.82
Coeff. Variation	0.46	0.60	0.97	0.44
Kurtosis	4.56	42.39	38.81	4.10
Skewness	1.26	6.05	5.82	0.92

Table 7. Summary univariate statistics for Cd, Cu, Pb, and Zn metal concentrations at an average depth of 30-in at the DWMA (n = 56). Dimensions are mg/kg except for coefficient of variation, kurtosis, and skewness, which are dimensionless.

Statistic	Cd	Cu	Pb	Zn
Mean	31.66	79.24	149.53	1904.88
Median	29.48	77.83	127.87	1880.00
Minimum	3.56	21.88	33.62	266.55
Maximum	73.76	137.27	381.60	4620.00
Standard Deviation	20.44	20.70	69.86	1308.40
Coeff. Variation	0.65	0.26	0.47	0.69
Kurtosis	-1.50	2.19	1.20	-1.52
Skewness	0.22	0.13	1.07	0.19

Table 8. Summary univariate statistics for Cd, Cu, Pb, and Zn metal concentrations at an average depth of 39-in at the DWMA (n = 44). Dimensions are mg/kg except for coefficient of variation, kurtosis, and skewness, which are dimensionless.

Statistic	Cd	Cu	Pb	Zn
Mean	26.36	88.29	145.55	1607.49
Median	15.19	85.99	106.88	628.64
Minimum	1.24	20.40	24.70	171.10
Maximum	108.71	195.05	443.75	7300.00
Standard Deviation	27.67	32.00	96.33	1851.58
Coeff. Variation	1.05	0.36	0.66	1.15
Kurtosis	1.43	2.27	2.60	2.59
Skewness	1.53	0.95	1.80	1.82

We used analysis of variance to test the hypotheses that for each metal the mean value at an average depth was the same as the adjacent depth. Calculated F statistics (Table 9) demonstrate that there were significant differences ($\alpha = 0.05$) in the Cd and Zn mean concentrations between the 6- and 18-in depths and between the 18- and 30-in depths but not between the 30- and 39-in depths. In contrast, there was a significant difference in the mean Cu concentration only between the 6- and 18-in depths and in the mean Pb concentrations only between the 18- and 30-in depths.

Table 9. F statistic comparing mean metal concentrations at adjacent depths.

	F statistic for each comparison ($F_{critical,\ \alpha = 0.05} = 3.9$)			
Depths (in) Compared	Cd	Cu	Pb	Zn
6 and 18	10.9	5.3	3.1	15.2
18 and 30	21.9	3.0	6.6	22.9
30 and 39	1.6	2.5	0.1	1.2

The trend in concentration with depth is also shown in Figure 10. (To show all data conveniently, Figure 10 shows the mean concentration at each depth divided by the mean at the 6-in average depth.) This figure, in conjunction with the data in Table 9, demonstrate that there is a statistically significant decrease in mean soil Cd and Zn concentrations with increasing depth to the 30-in level. There are also variations in mean concentrations of Cu and Pb with depth, but the trend is not as consistent.

With these data it is possible to estimate the mass of each metal in soils at the DWMA. Based on the mean concentrations at each average depth and assuming a soil bulk density of 2.0 g/cm^3, most of the metals (Table 10) occur in the top 12-in of soil. Amazingly, there could be more than 2.3×10^6 lbs of Zn in the top foot of soil and over 5.0×10^6 lbs of Zn in the top three feet of soil at the DWMA.

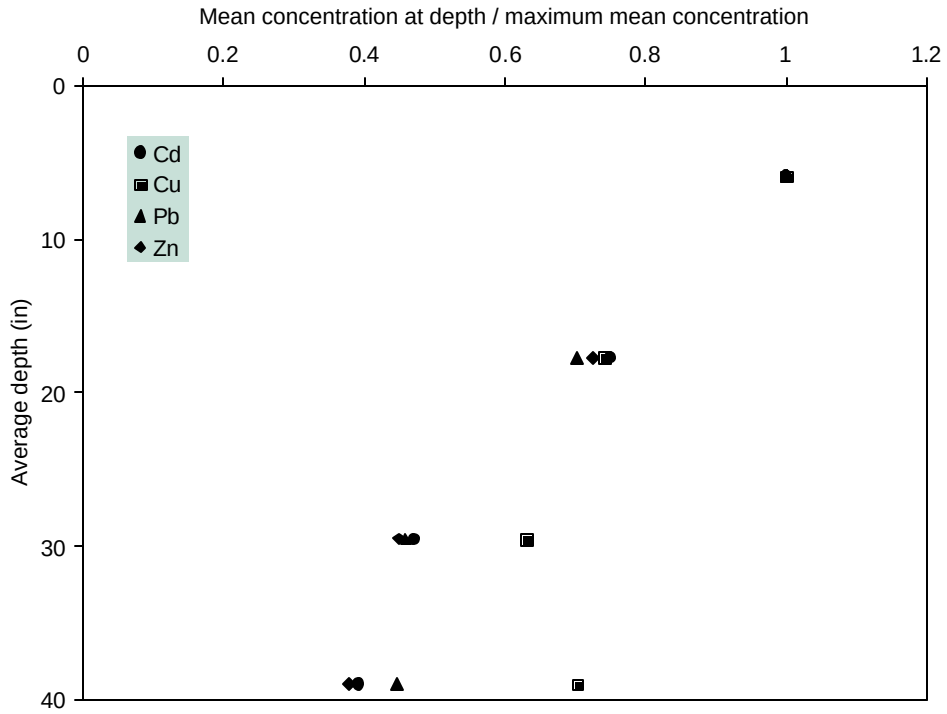

Figure 10. Normalized mean concentration of Cd, Cu, Pb, and Zn as a function of depth.

Table 10. Estimated total mass of each metal in the DWMA.

Average depth (in)	Mass (lb)			
	Cd	Cu	Pb	Zn
6	37,100	69,300	179,300	2,336,000
18	27,800	51,300	126,100	1,695,000
30	17,400	43,700	82,400	1,050,00
Total	82,300	164,200	387,800	5,081,00

Bivariate Description

The univariate statistics describing the shapes of the metal concentration distributions for the various metals suggest that the metals can be divided into two groups. One group includes Cd and Zn; although the magnitudes of their concentrations differ considerably, both distributions are relatively broad. The other group includes Cu and Pb, which have relatively narrow distributions. These observations are confirmed in scatterplots (Figure 11 and Figure 12) that show a remarkable correlation between the metal concentrations in each group. Consistent with the descriptions of their distributions, Cd and Zn concentrations cover a broad range, whereas Pb and Cu concentrations are bunched in narrow clouds that

stretch out to a few high values. Correlation coefficients for the Cu:Cd and Pb:Cd scatterplots (not shown) were 0.59 and 0.68, respectively.

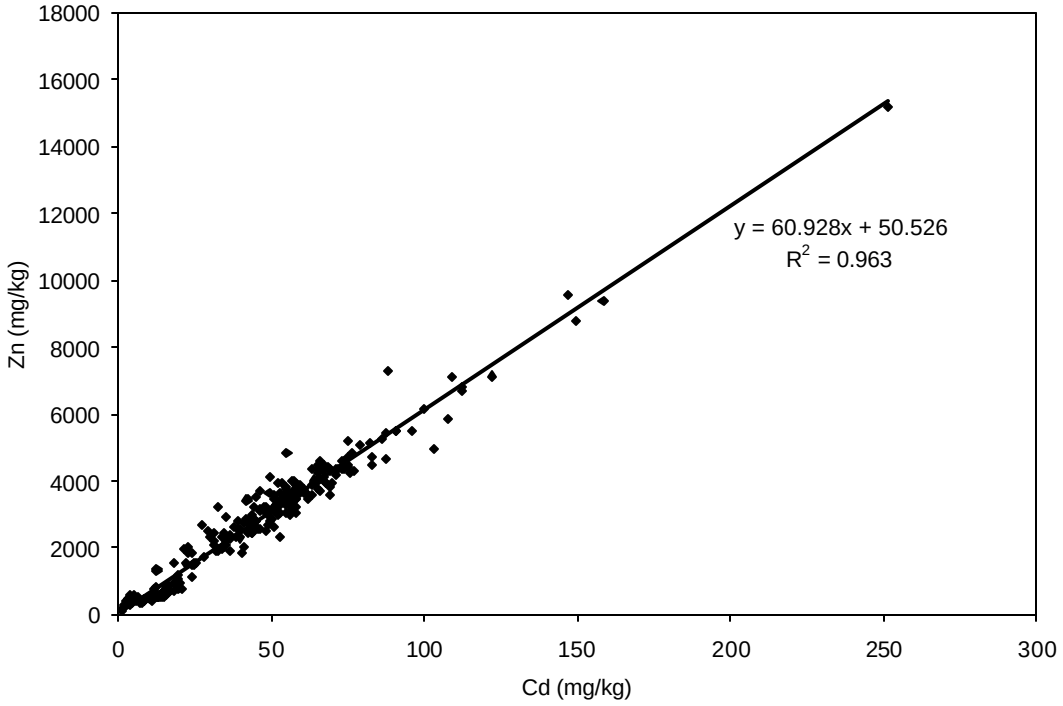

Figure 11. Correlation between Zn and Cd concentrations at the DWMA.

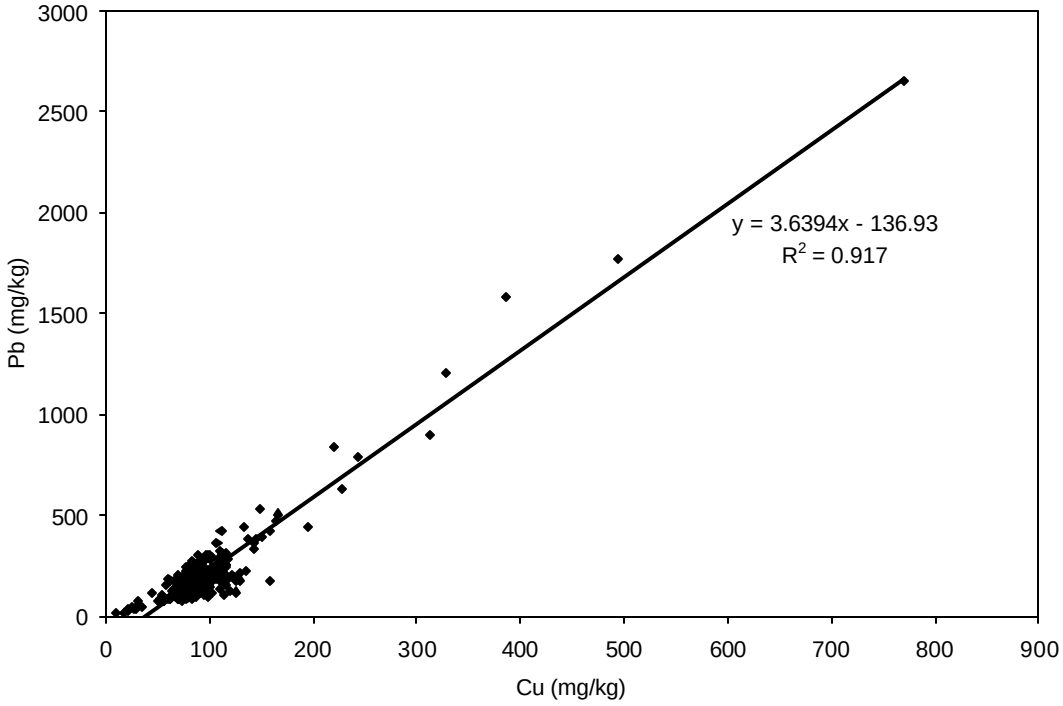

Figure 12. Correlation between Pb and Cu concentrations at the DWMA.

Soil Carbon Analyses

Soil carbon analyses were limited to 12 samples from among the cores collected. This subset, collected to include some spatial variation (horizontal and vertical), involved cores with a range of visual and textural properties. In the field log these samples were described using terms such as “clay”, “sandy”, “black”, “wet”, or “top soil”. Despite this range of characteristics, the total inorganic carbon (TIC) content remained very uniform both with depth and among the different types of samples (Figure 13). In contrast, results for the total carbon (TC) measurement ranged from 2.5% to 5.5%. The difference between the TIC and Total C ranges is due to organic carbon. Although TIC appears very constant across the DWMA, the organic carbon content ranges from about 1.8% to 4.8%.

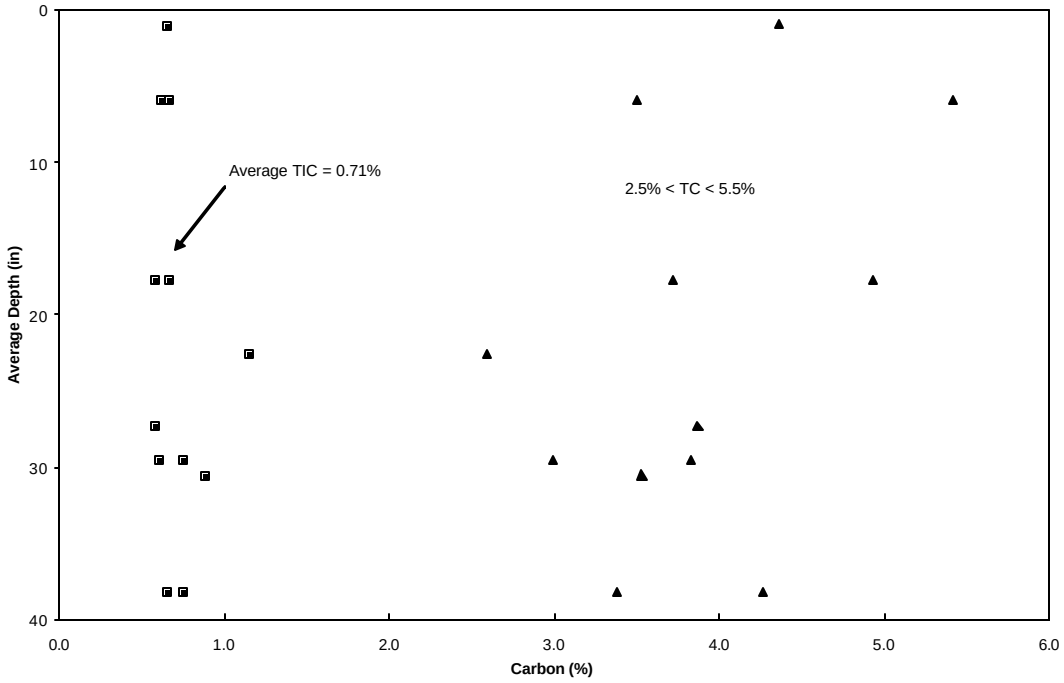

Figure 13. Changes in total carbon (triangles) and total inorganic carbon (squares) with depth. Data used to prepare this figure are in Appendix E.

Spatial Distribution of the Metals

This section includes representative qualitative contour maps of metal distribution and more quantitative maps prepared using ordinary block kriging.

Contour Maps

Contour maps showing interpolated metal concentrations across the site were similar for all metals at all depths. Sample contours maps for each of the average depths are shown in Figure 14 through Figure 16.

(These three examples were selected at random; all metals exhibit similar patterns). Maximum concentrations appear near the center of the northern boundary; minimum concentrations are typically near the southeast corner of the DWMA. There is no other structure or directional preference apparent in these maps.

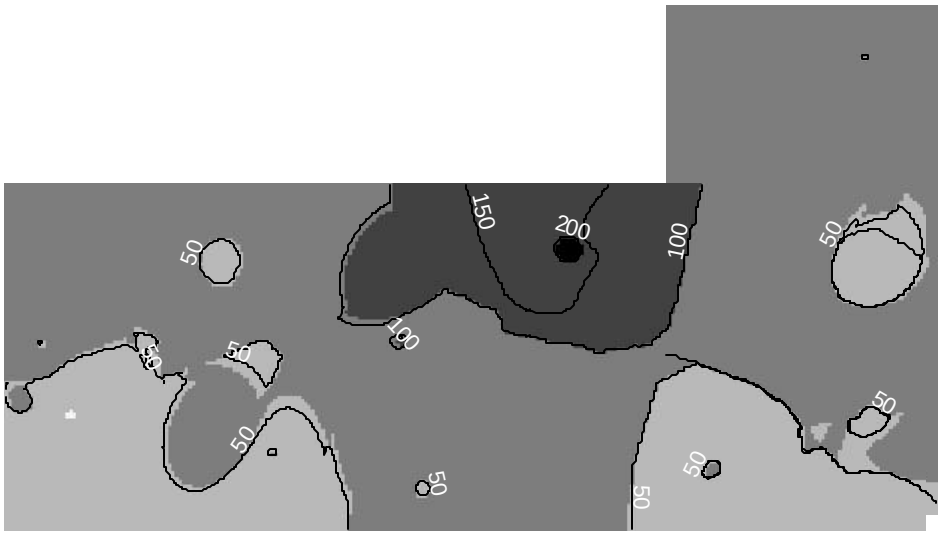

Figure 14. Contour map of Cd concentrations (mg/kg) at 6-in average depth.

Figure 15. Contour map of Zn concentrations (mg/kg) at 18-in average depth.

Figure 16. Contour map of Pb concentrations (mg/kg) at 30-in average depth.

An alternative interpolation scheme, which involves generating variograms, evaluating cross validation, and kriging, is presented in the next section.

Variogram Models

Variograms are used to quantify how pairs of metal concentrations change with the separation distance between them. Typically one or more members from a family of mathematical models are used to reproduce the trend observed in the data. Because of the limited amount of data (only four data points per variogram and a wide range in the lag distances), it was hard to justify using complex, multi-parameter models. Instead, we tried to represent the structure with only one mathematical model. The model type for each metal and the model parameters are summarized in Table 11.

Table 11. Variogram models and parameters for each metal at the 6-in average depth.

Parameter	Cd	Cu	Pb	Zn
Model type	Spherical	Gaussian	Gaussian	Gaussian
Nugget	10	1000	30000	600000
Sill	610	8000	80000	1800000
Range (ft)	95	80	80	95

The nugget represents a discontinuity at the origin of the variogram. This effect could result from short scale variability or sampling error. The range is the distance where the variogram reaches a plateau. Beyond the range the variance between sample pairs is a constant function of distance. The sill is the value the variogram reaches at the plateau. These features are readily seen in Figure 17 through Figure 20.

These figures demonstrate that there is spatial continuity in the distribution of metals at the DWMA. The variance between concentrations is relatively low at short distances and it reaches a constant level at a distance (range) between 80 and 95-ft. Variograms for Cd, Cu, and especially Pb show a depression or hole effect around 26-ft. If this effect is real, it suggests that relative to the sample pairs separated by about 7-ft, there is less variance between sample pairs separated by about 26-ft. Alternatively, this effect could be an artifact resulting from erratic data. It is possible, for example, that one sample pair has an unusually large variance among sample pairs in the shortest lag. Upon inspection of the data, however, there was no justification for removing specific data from the evaluation.

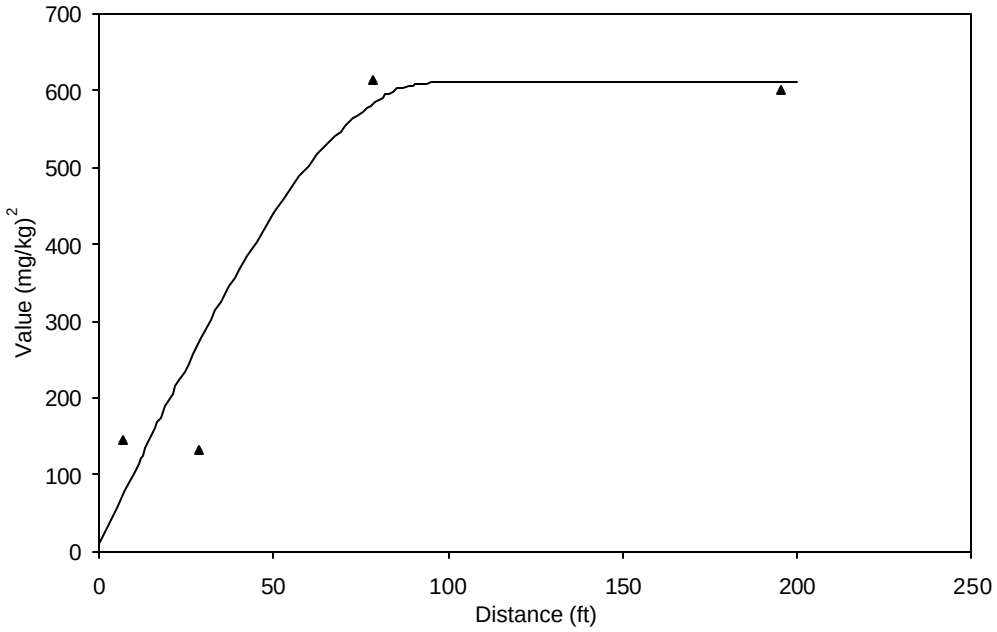

Figure 17. Variogram and data for Cd at 6-in average depth.

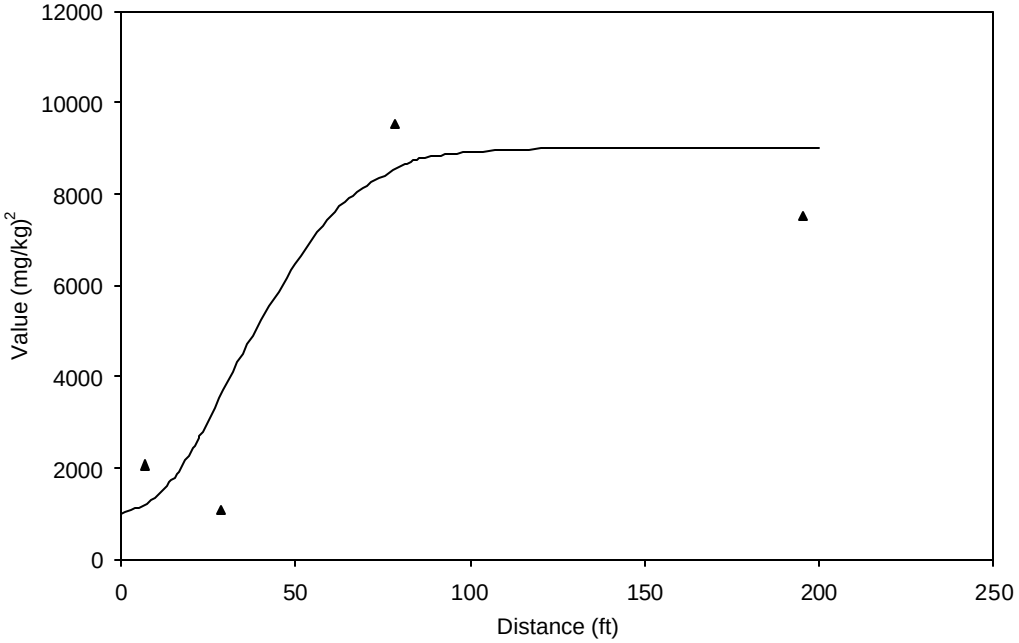

Figure 18. Variogram and data for Cu at 6-in average depth.

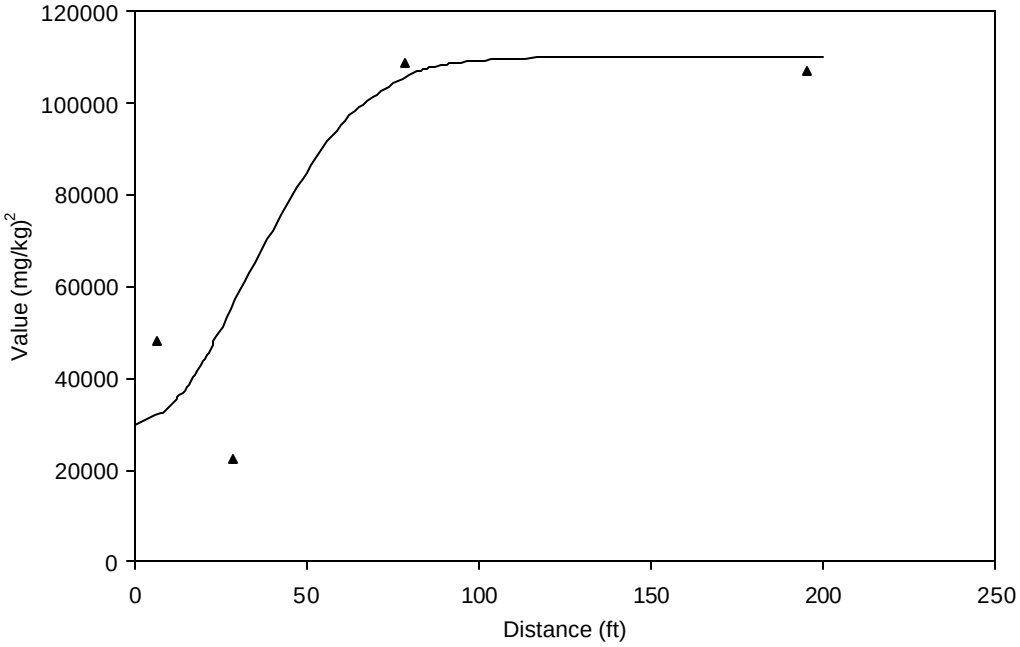

Figure 19. Variogram and data for Pb at 6-in average depth.

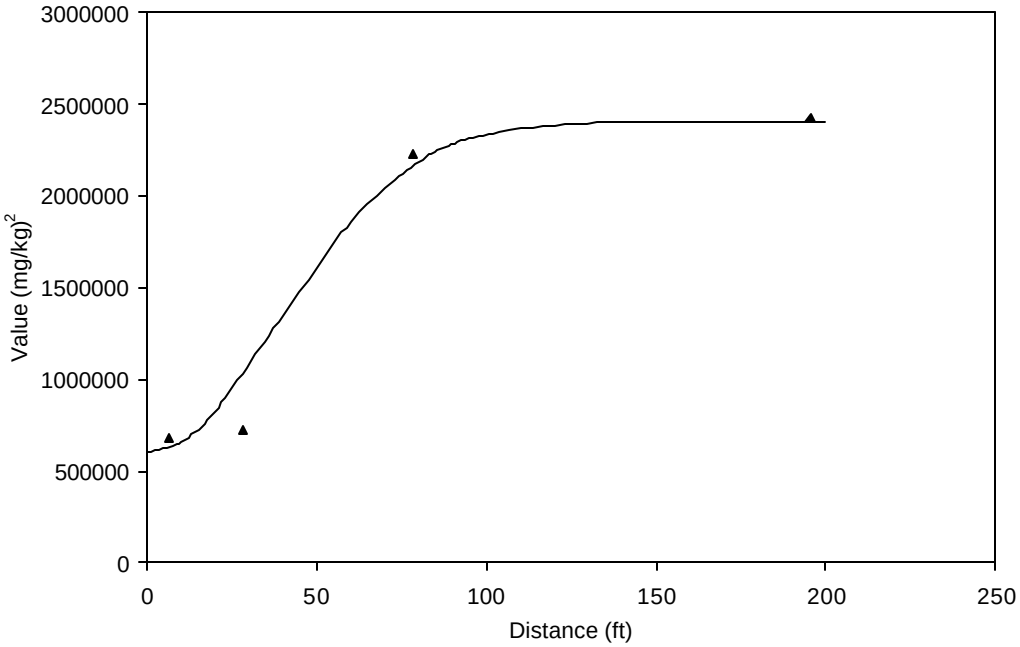

Figure 20. Variogram and data for Zn at 6-in average depth.

Variogram analysis at other average depths was more problematic. For example, relative to the 6-in average depth level, variogram data for Zn at the 18-in average depth level (Figure 21) are more erratic.

One explanation of this observation is that metal concentrations are more uniform and there is little spatial continuity in the data at the other depths. Alternatively, whereas a single model could fit the variograms at the 6-in average depth, more sophisticated approaches could be needed for the other sample depths. Some of these other approaches include eliminating erratic data from the analysis, working with linear combinations of variogram models, or considering other measures of spatial correlation such as a relative variogram or a directional variogram. Initial assessment of some of these options, however, suggested that there were not enough data to justify these adjustments. Therefore, the following sections deal with kriging applied to the 6-in average depth only.

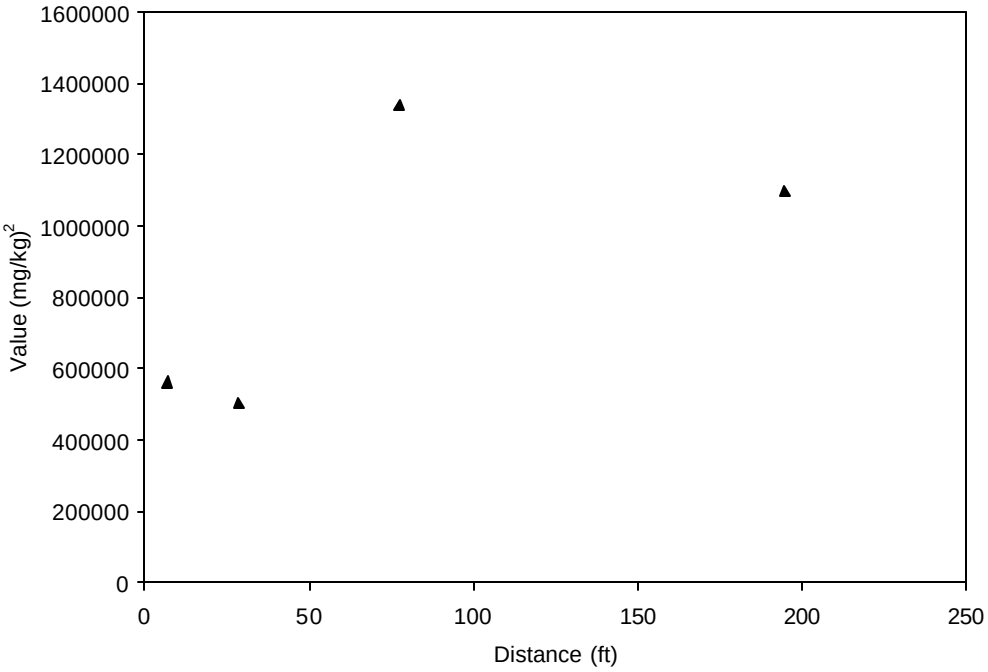

Figure 21. Variogram data for Zn at 18-in average depth.

Cross Validation

One way to assess the accuracy of the variogram model is through a cross validation exercise. In cross validation, a measured value at one location is removed from the sample population and the remaining data are used to estimate the missing value. This process is repeated for the entire data set. Scatterplots comparing estimated and measured values for each metal are shown in Figure 22 through Figure 25. The solid line in each figure represents perfect correlation between the estimated and measured concentrations. Data points in these figures appear to be symmetric with respect to the line; there is no obvious bias in the estimates. Agreement between estimated and observed concentrations, however, is better at lower concentrations; the greatest errors occur in estimates at relatively higher concentrations.

Estimates for Cu and Pb especially suffer at the highest concentrations. Another problem with the estimates for Pb is that one of the estimated concentrations is negative. This result, an artifact of the interpolation algorithm, is obviously impossible and should be manually reset to 0. Correlation coefficients for these cross validation data (Cd $r^2 = 0.72$; Cu $r^2 = 0.54$; Pb $r^2 = 0.35$; Zn $r^2 = 0.77$) provide a quantitative confirmation of information in these figures.

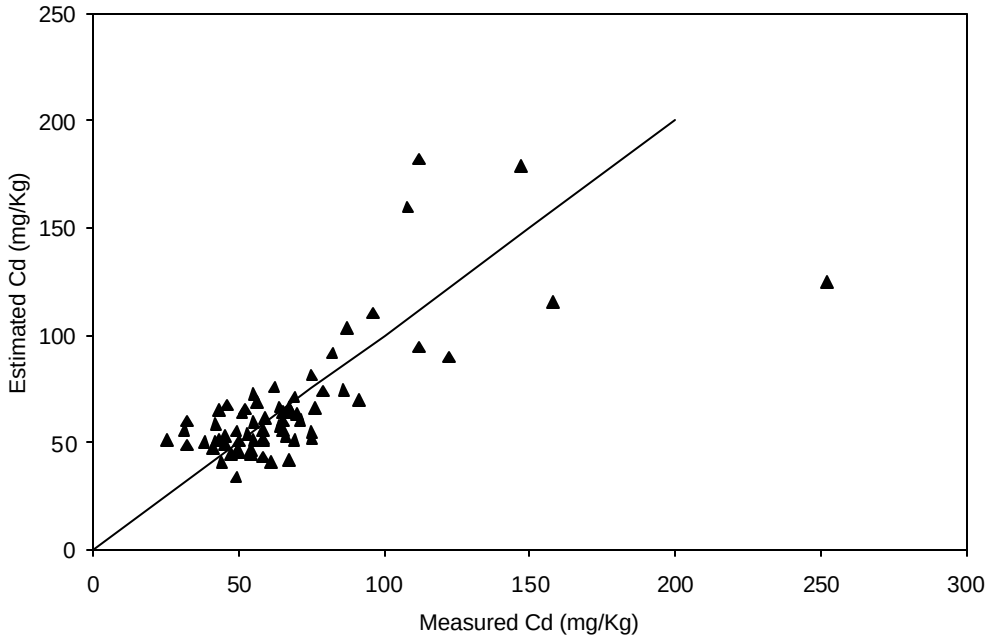

Figure 22. Cross validation scatter plot for Cd showing estimated concentration as a function of the measured concentration. Only data for the 6-in average depth were used.

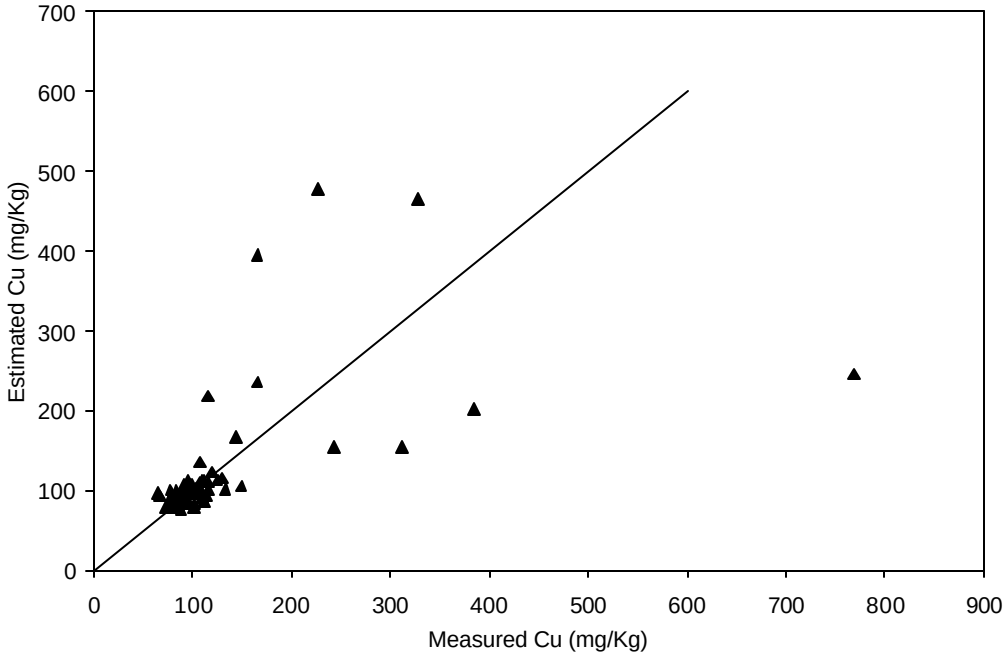

Figure 23. Cross validation scatter plot for Cu showing estimated concentrations as a function of the measured concentration. Only data for the 6-in average depth were used.

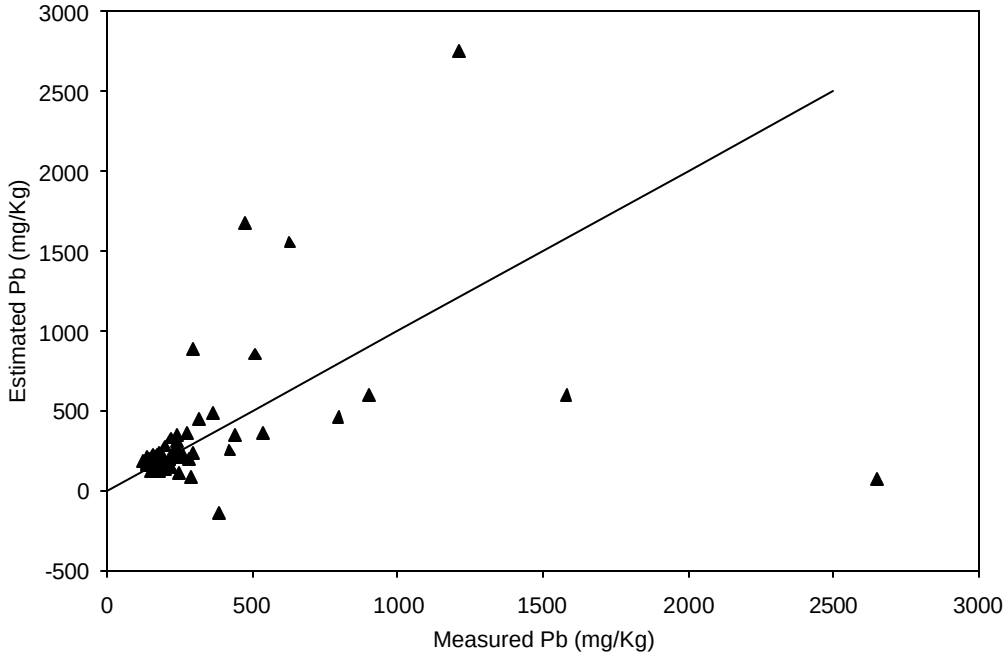

Figure 24. Cross validation scatter plot for Pb showing estimated concentration as a function of the measured concentration. Only data for the 6-in average depth were used.

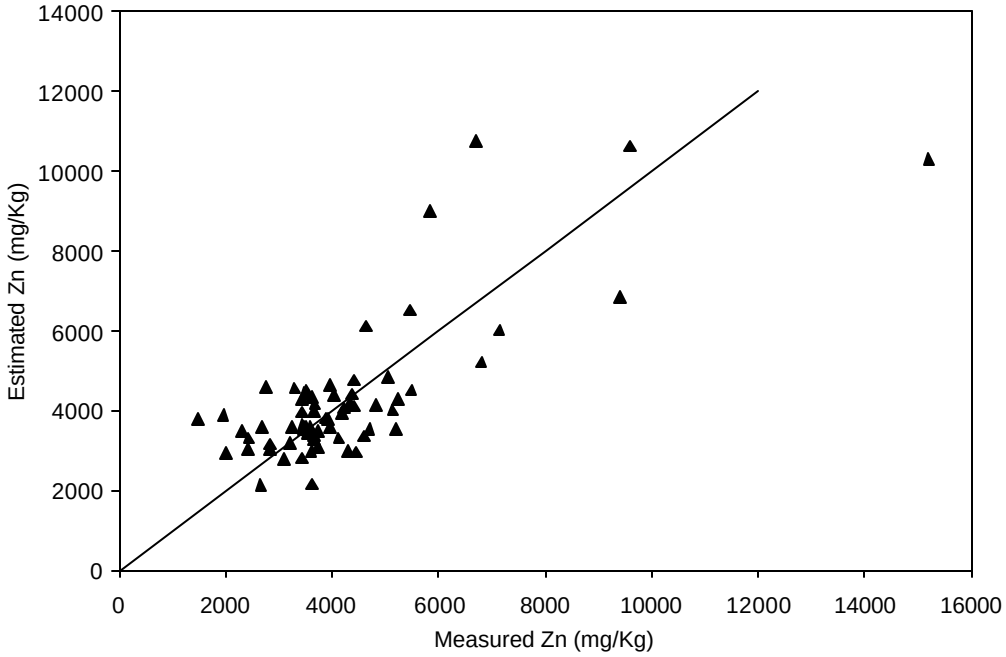

Figure 25. Cross validation scatter plot for Zn showing estimated concentrations as a function of the measured concentration. Only data for the 6-in average depth were used.

Ordinary Block Kriging

Variogram models described above were used in ordinary block kriging. Blocks were 50-ft by 50-ft, with a 4×4 grid of discrete points within each block. Search parameters for the interpolation process were: Radius = 400 ft, angle = 0, sectors = 1, maximum in sectors = 8, minimum to use = 1, and distance type = variogram. Results showing the interpolated concentrations for each block can be seen in Figure 26 through Figure 29.

The legend accompanying each figure defines the concentration range for each of four shades of gray. In each case, the population of estimated concentrations is divided approximately into quartiles so that each range represents one-quarter of the blocks. For example, the Cd distribution (Figure 26) shows a minimum estimated concentration of 28 mg/kg. About one-quarter of the total population of estimated concentrations lies in the narrow range from 52 to 58 mg/kg, and the last quartile includes the very broad range from 81 to 252 mg/kg. The darkest shade in these figures is labeled "Unknown" to represent blocks where there were not sufficient data to interpolate a value. This effect is mostly due to the limited number of samples in this initial survey. In these figures the highest concentrations for all metals begin near the center of the northern boundary and then trail off toward the southwest.

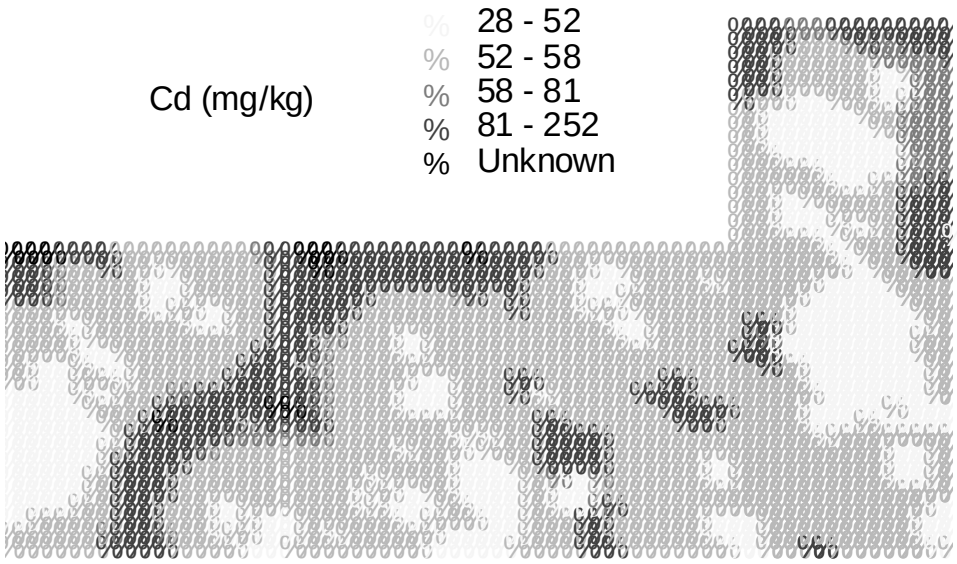

Figure 26. Block kriging interpolated soil Cd concentrations at the DWMA.

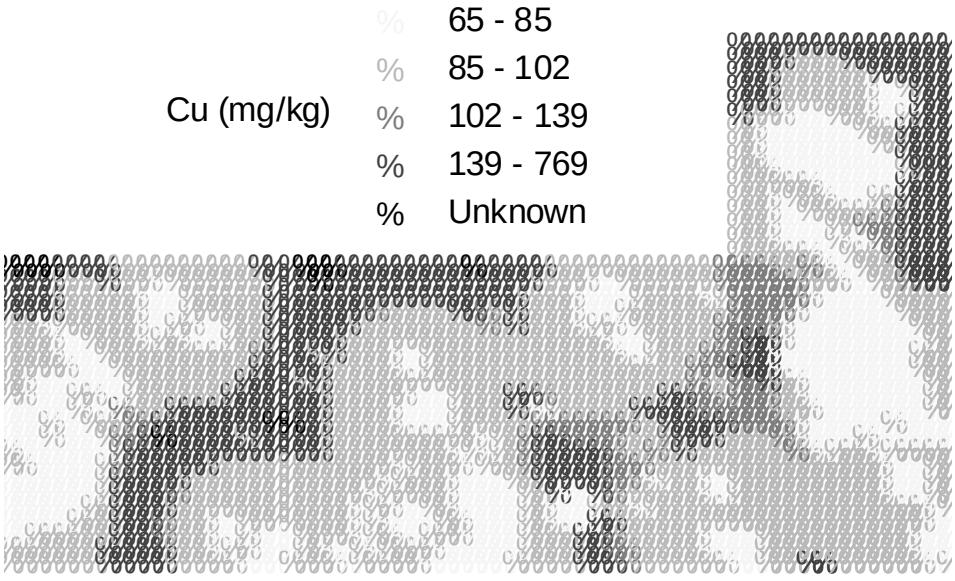

Figure 27. Block kriging interpolated soil Cu concentrations at the DWMA.

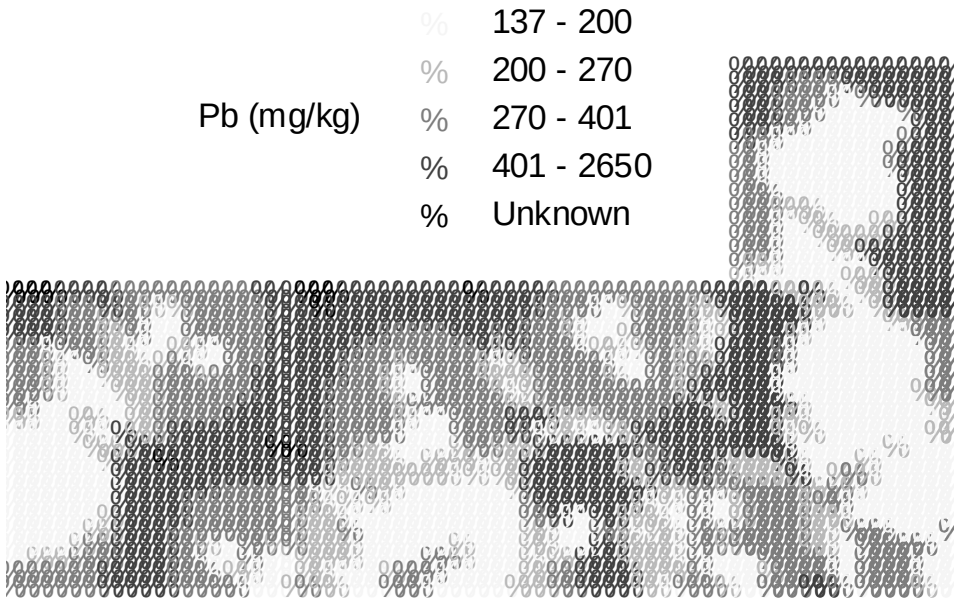

Figure 28. Block kriging interpolated soil Pb concentrations at the DWMA.

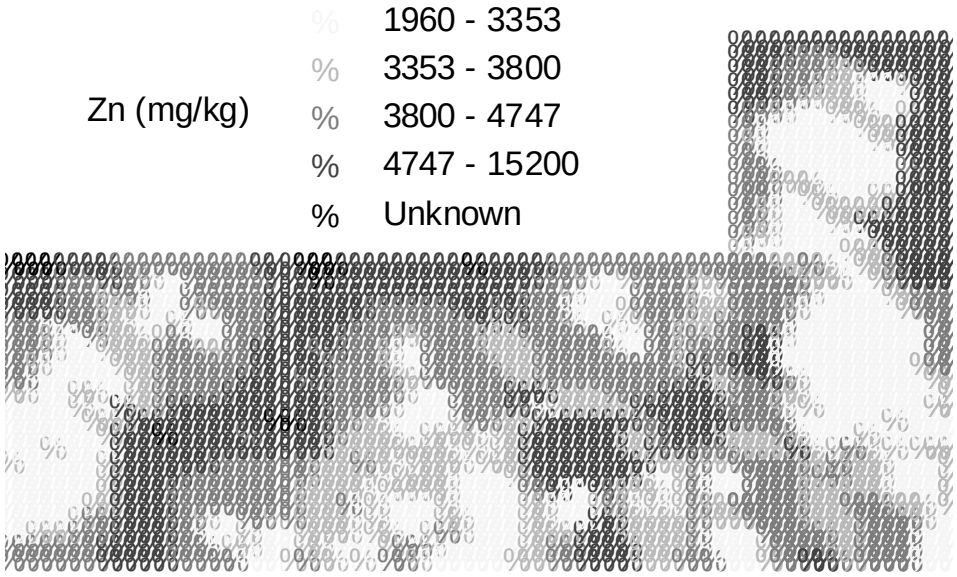

Figure 29. Block kriging interpolated soil Zn concentrations at the DWMA.

Kriging Standard Deviation

Estimated standard deviations for interpolated concentrations at the 6-in average depth are shown in Figure 30 through Figure 33. These figures follow the format used previously to represent the interpolated concentrations. Each shade of gray represents approximately one quartile, or one-fourth of the population of blocks. The darkest shade of gray in each figure shows blocks where there were not enough data to estimate the local standard deviation. In the case of Cd, for example, (Figure 30) the estimated uncertainty ranges from 6 to 32 mg/kg. Most of the uncertainty arises in the northern fringes and in a band stretching from the southwest corner to the middle of the northern boundary. About half the site has estimated errors less than 24 mg/kg.

Spatial Continuity Summary Comments

Interpolated metal concentrations presented above should be used carefully because they were developed using a limited amount of data from an initial site survey. The two different interpolation schemes (inverse distance weighting and kriging) do yield qualitatively similar results: Some of the highest metal concentrations appear near the center of the northern boundary and some of the lowest metal concentrations appear in the east and southeast sections. There are, however, marked differences shown in the details of the different contour plots. For example, although the regions of high metal concentration overlap, the highest concentration shown using inverse distance weighting appears to coincide with one of the low concentration regions in the plot generated from kriging.

Kriging provides useful information beyond the contour maps. For example, the variograms show that there is spatial structure to these data at the 6-in average depth but there may be little structure at greater depths. Variograms also provide a scale for that structure, which can guide future sampling efforts. The high correlation between metal concentrations at short distances decreases to a constant background level at separation distances of from 80- to 95-ft. Furthermore, results from kriging also suggest that relative errors associated with estimated concentrations are small for Cd and Zn, mid-range for Pb, and largest for Cu. Finally, in contrast with inverse distance weighting, kriging is perhaps more “honest” in that it clearly shows on the contour maps where additional data are needed. Some additional applications of kriging to management decisions are noted in the final section of this report, which focuses on recommendations.

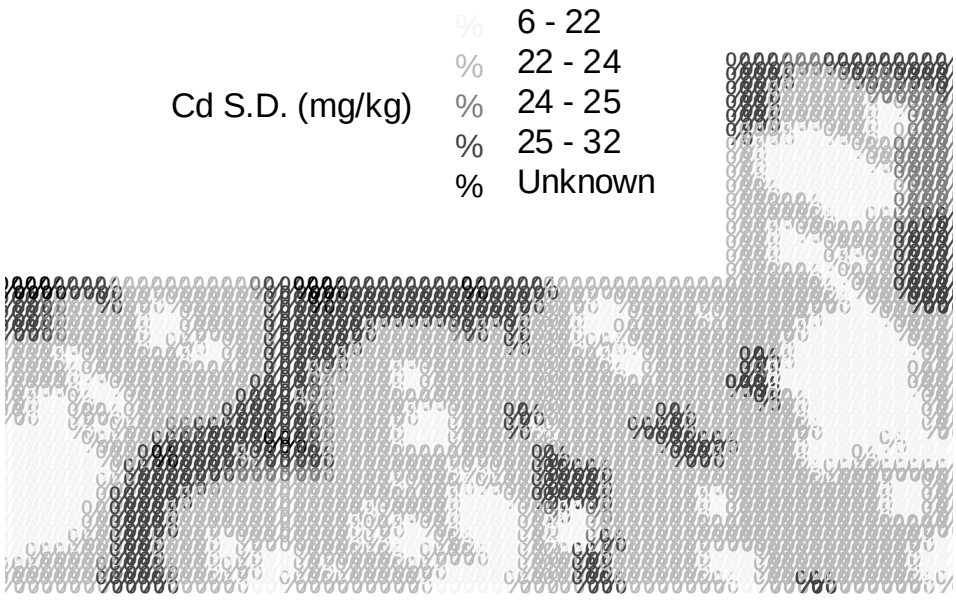

Figure 30. Kriging standard deviations for Cd concentrations at the DWMA.

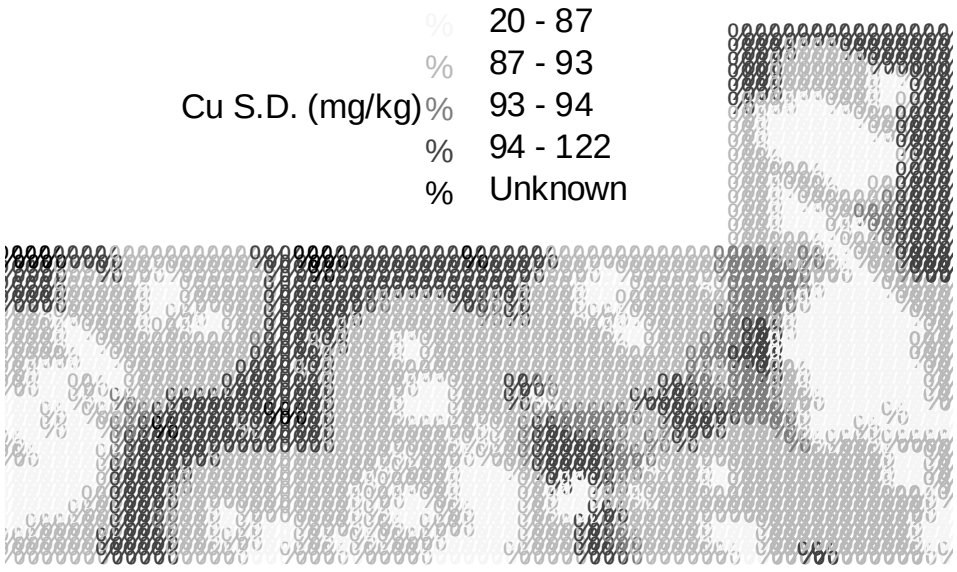

Figure 31. Kriging standard deviation for Cu concentrations at the DWMA.

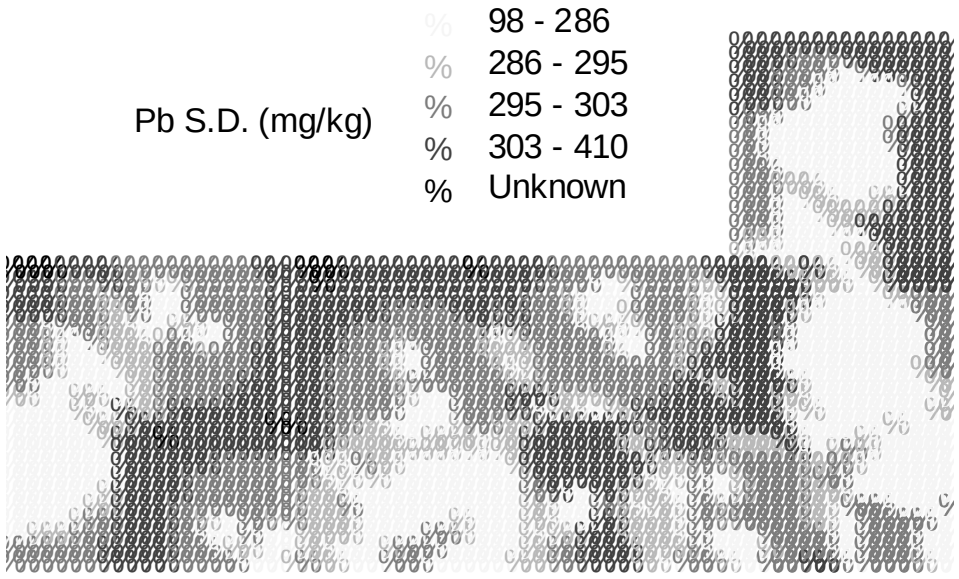

Figure 32. Kriging standard deviations for Pb concentrations at the DWMA.

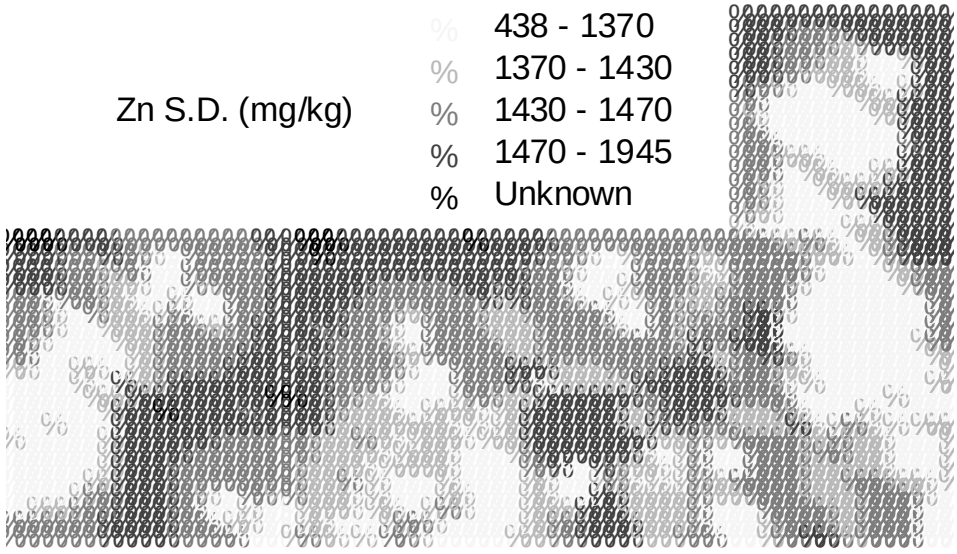

Figure 33. Kriging standard deviations for Zn concentrations at the DWMA.

Clay Minerals

Diffraction patterns from sample cores were very consistent (Figure 34). (In Figure 34 and Figure 35 amplitudes of the spectra were scaled to display all spectra within one figure. The absolute amplitude of the peak is not important.) All samples showed dominant and secondary peaks at 2Θ = 27° and 12.5°, respectively. Lesser peaks that were common to all samples appear at 2Θ = 45° and 17.7°. Core 4-58 had a strong peak at 2Θ = 31.6°; this peak was much smaller or not visible in the other samples.

Kaolinite, montmorillonite, and illite are common clay minerals in Illinois River sediment. Spectra for these reference clays (Figure 35) suggest that kaolinite and one or both of montmorilloinite and illite are present. Additional peaks showed up in the samples at 2Θ = 31.6°, 17.7°, and especially 45°; we have not been able to identify minerals responsible for those peaks.

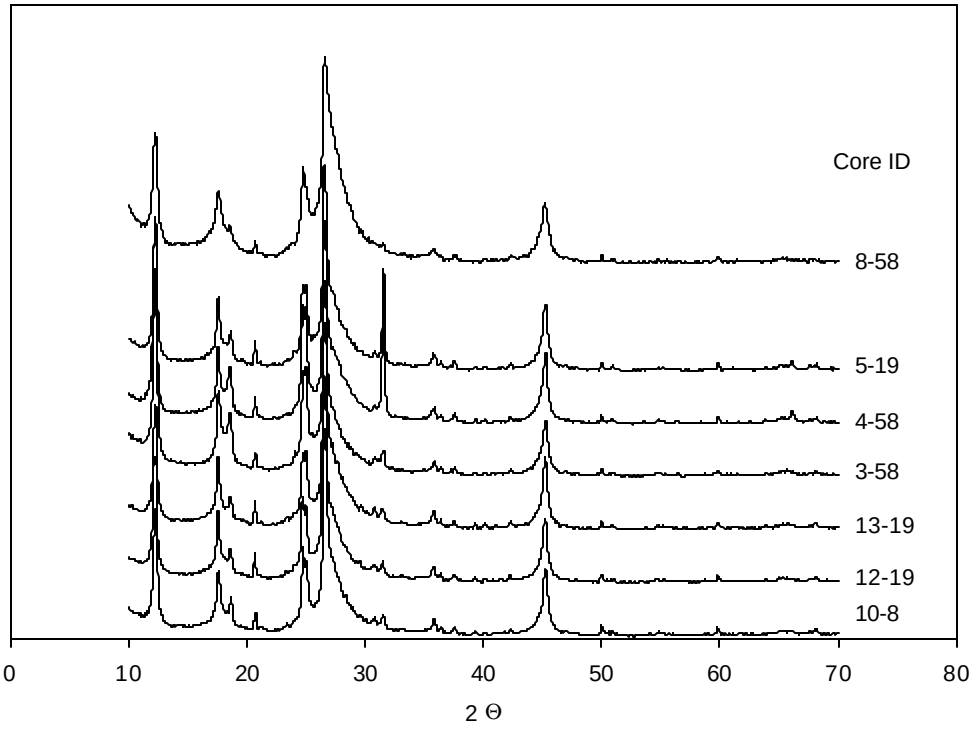

Figure 34. X-ray diffraction patterns from DWMA soil samples.

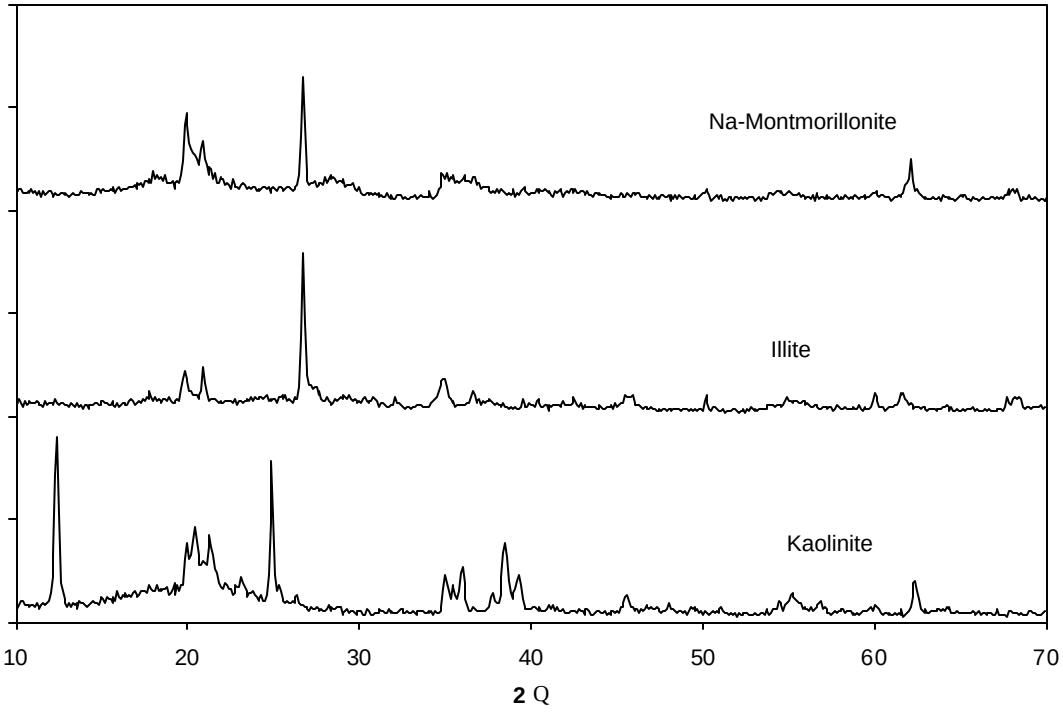

Figure 35. X-ray diffraction patterns for reference clays.

Metal Speciation

Extractions

Results from the extraction tests (Figure 36) reveal considerable variety in speciation among the metals. Speciation should also have an effect on metal mobility. The exchangeable fraction is probably the most mobile fraction; changes in the groundwater composition, due to flooding for example, could release metals from this fraction. Carbonate and Fe & Mn oxide fractions could also be relatively mobile. Carbonate-enriched phases could dissolve when the groundwater composition changes. If flooding and biologic activity create anaerobic conditions, the Fe & Mn oxide fraction could also dissolve. Metals species with the least mobility are probably tied up in organic matter and in the residual fraction. Based on these results, we expect metal mobility at the DWMA to be in the sequence: Cd > Zn > Pb > Cu.

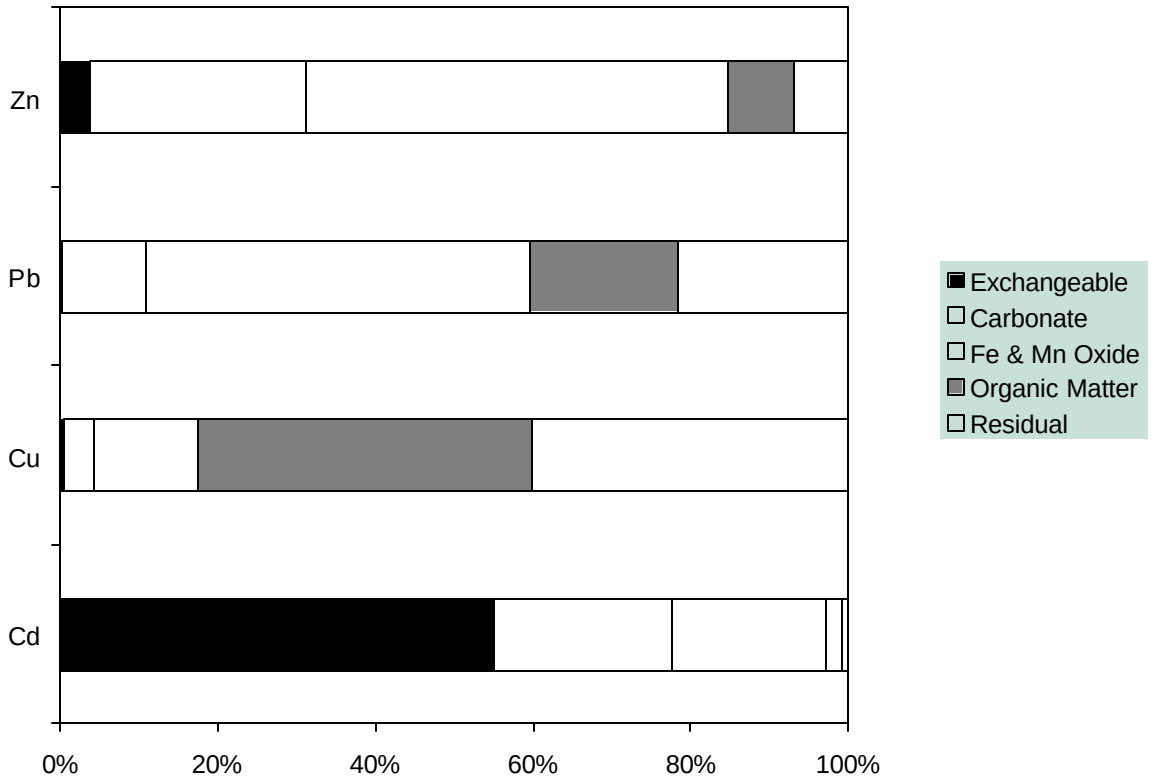

Figure 36. Metal speciation based on extraction tests; 12 soil cores were extracted. Data used to prepare this figure are in Appendix D.

XAS

This section begins with a discussion of problems encountered with Cd, Cu, and Pb analyses, along with some of the recent developments that can overcome those problems in future studies. Spectra obtained from Zn measurements and our interpretation of those results is also presented.

Problems and Potential Solutions for Cd, Cu, and Pb Analysis

Several different problems were encountered during our attempts to measure XAS spectra for Cd, Cu, and Pb. Some of the difficulties with these measurements arose because of their relatively low concentrations, the high intensity of the x-ray source, noise generated from the sample matrix, and limitations of conventional detectors. In XAS measurements, x-ray absorption by the target element produces secondary x-ray fluorescence; the intensity of this fluorescence is measured to monitor the XAS as a function of energy. Scattered radiation and fluorescence from other elements in the sample matrix produce an undesired background signal that, depending on the relative concentrations, can be much stronger than the desired signal. This background noise is typically the dominant source of noise in XAS measurements. The intense x-ray beams produced by third generation synchrotron sources such as the

APS can saturate conventional solid state detector arrays; these detectors are overwhelmed by the background noise.

These limitations are less pronounced for Cd, because it has a relatively high absorption edge energy (Table 12). As a result, relative to the other metals it is usually easier to distinguish the absorption spectra for Cd from the background noise. Unfortunately, for the duration of this study, the beam available at MR-CAT or Bio-CAT was not stable enough to take reliable XAS measurements at the high energy.

Table 12. Critical x-ray absorption energies for Cd, Cu, Pb, and Zn.

Element	Edge Energy (keV)	Edge
Cd	26.71	K
Cu	8.98	K
Pb	15.86	L_1
Zn	9.66	K

One approach to dealing with background noise is to eliminate it before it gets to the detector. A new technology that appears well suited to this task is the Multilayer Array Analyzer Detector (MAAD). The MAAD uses diffraction (in the Bragg geometry) from an array of graded d-spacing synthetic multilayers to select the desired x-ray fluorescence and reject the rest. This device works well below about 13 kev but loses efficiency at higher energies. Two MAADs working together are comparable in performance and cost to a conventional 13 element germanium detector, but the MAAD effectively has no count rate limitations.

Another approach, which is most appropriate above 13 kev, is the Bent Laue Analyzer. This analyzer relies on Bragg diffraction from a thin silicon crystal in the Laue geometry (in which the x-rays are transmitted through the crystal). The crystal is bent to a specific logarithmic spiral shape so the diffraction condition is met everywhere on the crystal. The extreme bending changes the diffraction properties of the crystal, effectively increasing its diffraction width by a factor of 10 to 20. The "forgiving" nature of these devices greatly improves their efficiency. Although originally designed for higher energies, Bent Laue Analyzers have been successfully tested below 10 kev, where they offer the unique advantage of high energy resolution at the lower energies.

Problems encountered attempting to measure Cd, Cu, and Pb at the DWMA were part of the inspiration driving the development of these new detectors. Unfortunately, neither the Bent Laue Analyzer nor the MAAD were available during the span of the DWMA study.

XAS Analysis of Zn

Absorption spectra for Zn from several different soil cores and different vertical positions at the DWMA are shown in Figure 37. (In Figure 37 although the vertical axis shows absorption the units are arbitrary; the spectra have been scaled so that several different curves could be shown in one figure). It is clear from these spectra that there was little variation in Zn speciation either from core-to-core across the DWMA or with changes in depth. To describe that speciation, it is necessary to interpret the sample spectra in terms of spectra from the standards (Figure 38). Results from the linear programming fitting procedure suggest that the dominant forms of Zn are $ZnSO_4$(s) and $ZnCO_3$(s). Although the presence of $ZnCO_3$(s) is in agreement with the extraction tests, it is surprising that $ZnSO_4$(s) should be an important species. It is also surprising that Zn adsorbed to clay and especially Zn adsorbed to hydrous ferric oxide, are not significant. There are at least two reasonable explanations for this surprising XAFS interpretation of the dominant forms of Zn.

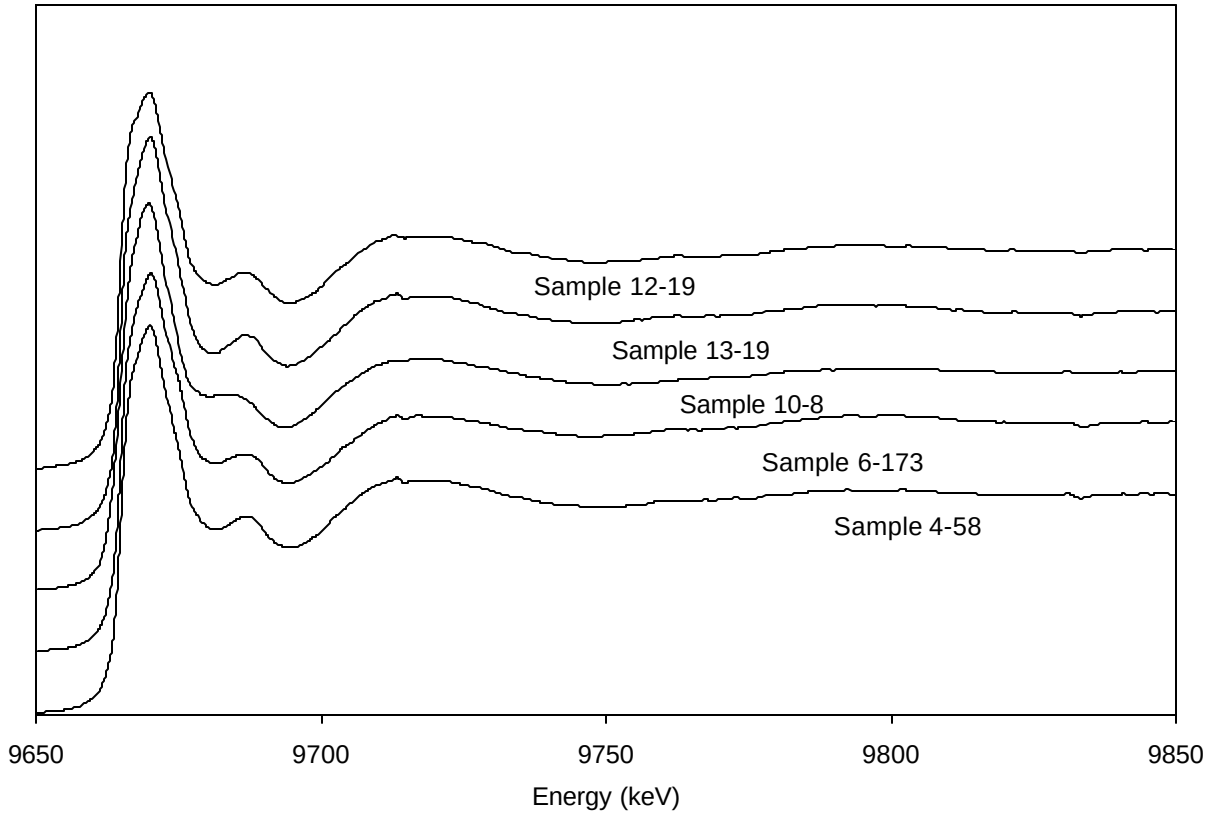

Figure 37. XAS spectra for Zn from different soil cores at the DWMA.

One explanation has to do with the set of standards that make up the basis set. Predicted speciation is only as good at the basis sets that are available; incomplete basis sets can produce unpredictable errors. For complex systems such as soils, a complete basis set or library of standards should be developed.

Minerals that make up the standards should be selected from XAS microprobe analysis of elements found near the specific target element, in this case Zn.

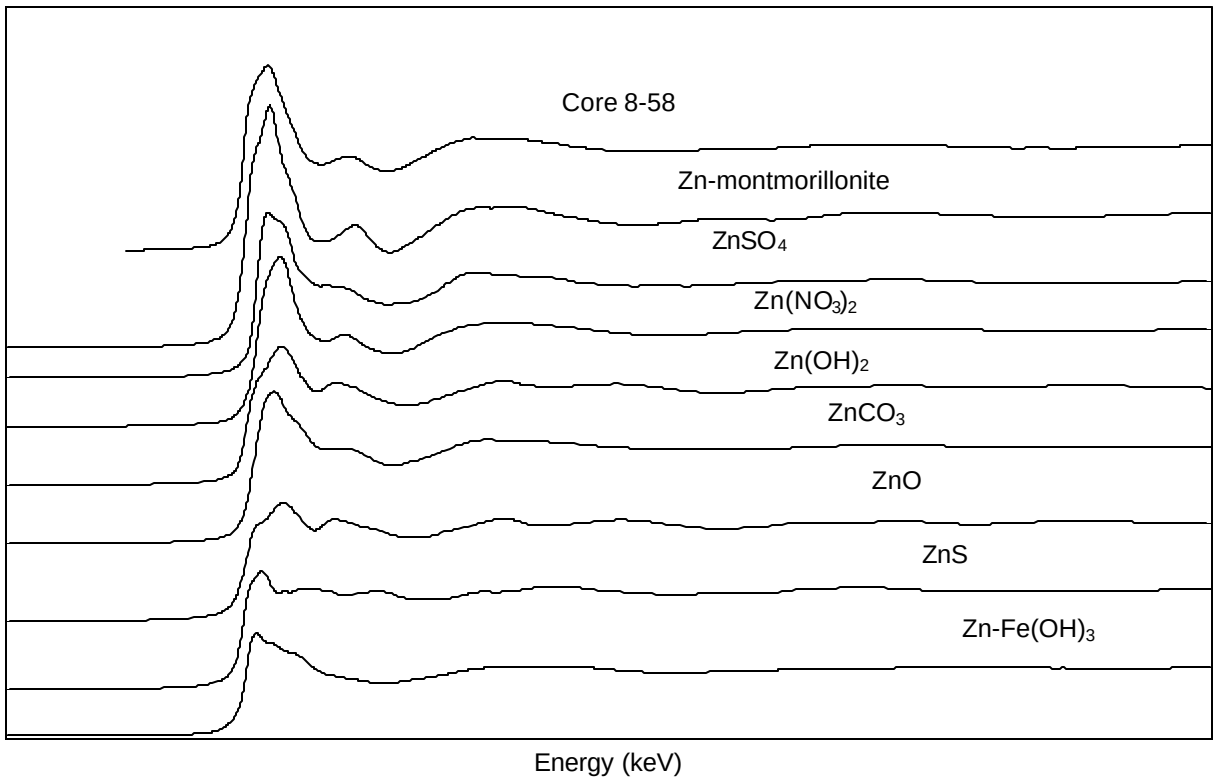

Figure 38. XAS spectra for one core and the standards used in the Zn analysis.

Another explanation for the unexpected result involves particle size effects. At the energy used to measure Zn spectra, the absorption length of the Fe oxide phase is approximately 10 to 20 μm. If primary or aggregated particles are large relative to the absorption length, much of the Zn on the interior of the particle would be invisible to the x-ray beam. One way to work around this limitation would be to grind the sample to insure that the particles are small relative to the absorption length. Alternatively, a technique called resonant x-ray inelastic scattering could be used. This technique provides XAFS spectra of a low energy edge while measuring at high energies. Briefly, when an intense, high-energy beam penetrates the sample, inelastically scattered x-rays can be observed using appropriate crystal optics. Because the incident and scattered x-rays are both at high energies, particle size effects are irrelevant. Although this technique is relatively insensitive, the high flux of the undulator beamlines at the APS should be sufficient to compensate for the loss of signal.

Chapter 4. Discussion

In this section we attempt to weave the results together to form a consistent pattern, develop a conceptual model that fits that pattern, and discuss the implications of the results.

Towards a Consistent Picture

Based on conventional statistics, the population of metal concentration measurements can be divided into two types of distributions, one for Cd and Zn and one for Cu and Pb. Although their individual values are different from each other, shapes of the population distributions for Cd and Zn are similar. This similarity is reinforced by the very high correlation coefficient ($r^2 = 0.96$) between these two parameters. It is also consistent with the observation that most of the Cd (95%) and Zn (83%) are associated with soil fractions (exhangeable, Fe & Mn oxides, and carbonate) that suggest greater mobility.

Likewise, the population distributions for Cu and Pb were similar to each other and there was a high correlation coefficient ($r^2 = 0.92$) between those two parameters. Speciation results suggest substantial association for Pb (45%) and Cu (80%) with soil fractions (organic, residual) that are probably not very mobile.

The comparison of means supports these differences. There are statistically significant differences in the mean concentrations of Cd and Zn in the upper layers of the soil and the trend indicates that concentrations decrease with depth. In contrast, significant differences between mean concentrations of Cu and Pb at adjacent depths are much more limited and not as consistent.

Finally, although the spatial interpolation presented here is based on limited data, the results are consistent. Despite substantial differences in the concentrations of the various metals, horizontal distributions of the concentrations were similar for all metals. The highest concentrations typically stretch from near the middle of the northern boundary toward the southeast. Lowest concentrations occur in regions near the east and west boundaries. Most structure in the spatial continuity occurred in the upper soil layers. Below the 6-in average depth, it was more difficult to assign variogram models to the data, suggesting that metals concentrations were more homogeneous in the deeper soils.

There are at least two ways to interpret the information from the DWMA. One scenario involves relatively immobile metals such that their current distribution represents the sediments as they were originally deposited at the DWMA back in 1982. It seems logical that deeper and older sediment in Lake DePue had the highest metal concentrations. When sediments were dredged from the lake and deposited in the DWMA, the sequence could have been reversed so that relatively uncontaminated sediment was on

the bottom and the more contaminated sediment was on the top. There are, however, several problems with this theory.

One problem is that the sediments were probably fairly well mixed during dredging and disposal. When sediments were pumped into the DWMA and prior to drying and consolidation there would have been ample opportunity to form much more homogeneous slurry than seen in data presented here.

Another problem stems from the fact that other researchers (Karny et al., 1997; Wehrmann, 2001) report small but detectable concentrations of metals in groundwater at the DWMA. The presence of soluble metals indicates that metals can be transported with moving groundwater.

Finally, the DWMA is subject to a variety of physical, chemical, and biological processes (many related to planned and accidental flooding) that continually alter their environment. It is difficult to believe that concentration gradients and similar distribution patterns established some 20 years ago could persist in such a dynamic system. It is more likely that these patterns exist because of, rather than despite, changes in the system. The next section includes a conceptual model that appears to be consistent with these patterns.

A Conceptual Model

A likely mechanism for metal movement involves periodic flooding of the DWMA. Either because of natural floods or due to the annual fall flooding in preparation for duck hunting, soils at the site are periodically underwater. Once submerged, microbial activity in the soil probably depletes the dissolved oxygen, creating anoxic conditions. Under these conditions, metals associated with certain soil fractions will be released into solution. The most important soil phase is probably the Fe and Mn oxide fraction, which is relatively soluble under anoxic conditions. Other soil fractions that could also release metals include the exchangeable fraction and, depending on the solution chemistry, the carbonate fraction. In contrast, metals associated with the organic and residual soil fractions are probably not very mobile.

Once released into solution, soluble metals would be transported along with the groundwater flow until conditions were right to react and attach to soil surfaces again. A fraction of these soluble metals probably react with clay minerals, forming a relatively exchangeable phase with the clay surface. This sequence of adsorption and desorption reactions with clay mineral surfaces retards the movement of metals relative to the groundwater velocity. As water levels within the DWMA drop and oxygen is once again available, dissolved Fe and Mn will precipitate. These freshly formed Fe and Mn oxides have a strong affinity for metals such as Cd, Cu, Pb, and Zn, and it is likely that a large fraction of the metals in solution become concentrated in these oxide solids.

This scenario points out ample opportunity for mobilization of metals within the DWMA. If biogeochemical processes are limited to metals leaching from the DWMA to the underlying groundwater, then this scenario is adequate. However, as noted above, data suggest that metals at the DWMA have become more concentrated in the surface levels. Therefore, what is missing from the processes outlined above is a mechanism to move metals from deep in the soil column towards the surface. Obvious choices include diffusion and advection, but neither one of these seems appropriate. Not only is molecular diffusion too slow (with effective diffusivities less than 10^{-6} cm^2/s it would take hundreds to thousands of years to transport metals to the upper soil layers), but diffusion processes work to remove rather than establish concentration gradients. Advection with the groundwater seems counterproductive because after a flooding event, groundwater flow will be down and out of the DWMA toward Lake DePue and the Illinois River (Wehrmann, 2001).

In the early stages of a natural flood event, however, water must accumulate outside the DWMA. If the flood level is high enough, the water will ultimately flow over the dikes onto the site. Until the flood reaches that level, the hydraulic gradient moves water through the dikes surrounding the site and up through the soil in the DWMA. Periodic natural flooding, therefore, provides a mechanism for advective transport of dissolved metals up through the soil column.

In this scenario, the horizontal distribution of metals reflects the relative height of soils in the DWMA. Higher elevation areas are flooded less frequently, and therefore have fewer opportunities to become enriched with metals. Low-lying areas, in contrast, have metal-enriched groundwaters flowing into them more often. Similarities between the interpolated maps of metal distribution and surface elevation are reasonably consistent with this model.

Water, of course, does not only seep into the DWMA. After natural floods, after flooding for duck hunting, and after precipitation (rain events and snow melt), the groundwater gradient is reversed and the flow is down and away from the site. These waters, however, originate at the surface and probably begin their journey with a relatively high concentration of dissolved oxygen. As a result, metals that have become associated with oxide minerals in the upper soil layers have less opportunity to be mobilized. Because waters seeping into and out of the DWMA have different characteristics, metal transport is asymmetric. In general, metals become relatively enriched in the upper layers of the soil. These effects are more noticeable at lower elevations because these regions are submerged more often. Finally, the effects are also greatest for the most mobile metals. Therefore, vertical concentration gradients are most noticeable for Cd and Zn, and much less for Cu.

This conclusion does not mean that there is no transport of metals away from the DWMA. Each time the site is flooded, some of the metals released from the deeper soil layers will not be transported all the way

to upper soil layers. When the hydraulic gradient is reversed and groundwater flow is away from the site, metals in solution will move in the same direction as the groundwater. Once again, relative to the groundwater velocity, the velocity of the metals will be slowed as a result of adsorption-desorption reactions with clay minerals. Speciation results from this study suggest that the relative mobility of metals away from the site should follow the sequence Cd > Zn > Pb > Cu. In the soils between the DWMA and Lake DePue or the Illinois River there should be concentration gradients reflecting this relative mobility.

Implications

The conceptual model developed here should be incorporated into a risk assessment for the DWMA. A critical part of the risk assessment involves metal concentrations at the site and how they compare with typical background exposure levels. Baker and Chesnin (1975) surveyed a variety of soils and reported mean concentrations and concentration ranges (Table 13); their data provide one way to assess typical background concentrations. Mean concentrations of these metals at the DWMA range from 4.7 times (Cu) to 90 times (Cd) these background values. Minimum metal concentrations observed at the DWMA are typically equal to or greater than the mean values reported by Baker and Chesnin. In terms of the maximum concentrations observed, Zn is remarkable; Zn concentrations can exceed 1.5% on a mass basis.

Table 13. Range and mean concentrations (mg/kg) from DWMA and a variety of soils surveyed by Baker and Chesnin (1975).

Metal	DWMA		Baker and Chesnin (1975)		Ratio of means
	Mean	Range	Mean	Range	
Cd	45	1 - 252	0.5	0.01 – 0.70	90
Cu	95	9 – 769	20	2 – 100	4.7
Pb	210	12 – 2,650	10	2 - 200	21
Zn	2772	112 – 15,200	50	10 – 300	55

Although the metal concentrations at the DWMA are clearly above “normal” background levels, this fact does not say anything about potential health effects. For more information, it is useful to turn to a study conducted by the Illinois EPA. In their summary fact sheet on the focused remedial investigation of sediment in the south ditch between the former New Jersey Zinc/Mobil Chemical site and DePue Lake, the Illinois EPA listed screening levels for two human risk assessment scenarios (ILEPA, 1998). These screening levels, which incorporate a number of assumptions about the pathway, duration, and frequency of exposure, are designed to identify when short-term exposure could pose an unacceptable human health

risk. The assumptions applied to that study might not be appropriate for the DWMA. Nevertheless, maximum concentrations of Cd and Pb at the DWMA do exceed the screening levels for construction workers, and the maximum concentration of Pb also exceeds the screening level for a child trespasser (Table 14).

Now that there is a better understand of the range of concentrations and the exposure pathways, human and ecological risk assessments could also be conducted for the DWMA.

Table 14. Maximum concentrations and screening levels for Cd, Cu, Pb, and Zn at the DWMA. Screening levels are described in a fact sheet on south ditch sediments (ILEPA, 1998).

Metal	Observed Maximum (mg/kg)	Screening Levels (mg/kg)	
		Child Trespasser	Construction Worker
Cd	251	1,200	200
Cu	769	47,000	8,200
Pb	2,650	400	400
Zn	15,200	350,000	61,000

Chapter 5. Conclusions

The objective of this study was to evaluate speciation and distribution of Cd, Cu, Pb, and Zn at the DWMA. Concentrations of these metals are at least four and as much as 90 times greater than their typical background concentrations in soils. Despite tremendous differences in their concentrations, the population distributions in this study fall into two groups. Concentrations of Cd and Zn are closely correlated with each other. These metals probably have the greatest mobility because of the soil fractions they associate with. Similarly, Cu and Pb concentrations are closely correlated with each other; their population distributions include more erratic, high concentration values. Lead and especially Cu have much less mobility because of the soil fractions they associate with.

All of the metals are probably influenced by changes in the environment and characteristics of the soil. The movement of water is an important factor in the movement of metals at the DWMA. When groundwater levels are rising, water percolates up and through the dikes into the soils where it first mobilizes and then transports metals. It is likely that Fe and Mn oxides play an important role in these processes. Under submerged, anoxic conditions, these oxides dissolve and their associated metals are also released into solution where they are transported along with the flowing groundwater. Although the metals move in the same direction as the groundwater, relative to the water velocity their transport is slowed as a result of sequential adsorption-desorption reactions with various soil fractions, especially clay minerals. When dissolved Fe and Mn come into contact with oxygenated surface waters, they can precipitate as oxide minerals. Some of the dissolved metals react with and become associated with these newly formed oxides.

As a result of these processes, the metals become more concentrated in the upper soil layers. Although each of the metals is somewhat affected by these processes, the effects are greatest for Cd and Zn, and least for Cu, because of their relative mobility. Despite the metal accumulation mechanism, it is likely that there is some transport of metals away from the DWMA toward Lake DePue and toward the Illinois River.

The spatial distribution of metals within the DWMA is consistent with this scenario. Vertical concentration gradients appear to be relatively steep for Cd and Zn, and shallow to non-existent for Cu. The horizontal distribution reflects the transport mechanisms; the highest concentrations of metals appear in the areas that are more frequently flooded.

Chapter 6. Recommendations

Further action at the DWMA should be planned in conjunction with a comprehensive risk assessment. One of the first questions to be addressed is: Given the current information, does the potential risk to humans and ecosystems justify a more thorough site assessment? For example, if screening levels developed for south ditch sediments are appropriate for the DWMA, then Cd and Pb concentrations in parts of the DWMA exceed the screening levels and remediation options need to be considered.

Although there are a large number of remediation options, likely scenarios include in-situ fixation, modifying the current operating procedures to minimize flooding, and soil removal. (A significant fraction of the total Cd is an exchangeable form. Remediation options for Cd should also consider extraction.) In each case, the geostatistical tools applied in this study can play an important role in subsequent site management decisions. For example, the block kriging estimates indicate that in the area around the north central boundary of the DWMA, the number of blocks that exceed screening levels for Cd and Pb are two and 351, respectively. The two sites for Cd are contained within the 351 blocks for Pb; in this case the risk assessment for Pb exposure determines the remediation response. To bring the DWMA into compliance with these screening levels, it would be necessary to remove 32,500 yd^3 of material.

Prior to any remediation action, it is important to understand the magnitude of the estimated errors and where those errors are greatest. The kriging estimates presented in this study shed some light on those issues. These estimates, however, should be used cautiously because standard deviations in kriging are sensitive to changes in the variogram model (Englund and Sparks, 1988). Furthermore, kriging standard deviations are usually not direct measures of local estimation accuracy (Deutsch and Journel, 1998). Isaaks and Srivastava (1989) suggest a method to scale the kriging standard deviation to the local uncertainty. Once more data are available, these and other stochastic simulation techniques (Deutsch and Journel, 1998) can be used to develop comprehensive remediation plans that consider both the economics of remediation and the relative risk.

Chapter 7. References

APHA (1995) Standard Methods for the Examination of Water and Wastewater 19th edition; edited by A. Eaton. L. Clesceri, A. Greenberg; American Public Health Association; Washington, D.C.

Baker, D.E.; Chesnin, L. (1975) " Chemical monitoring of soils for environmental quality and animal and human health" *Advan. Agron*. 27:305-374.

Brown, G.E. Jr. (1990) "Spectroscopic studies of chemisorption of reaction mechanisms at oxide-water interfaces" in *Mineral-Water Interface Geochemistry* edited by M.F. Hochella, Jr. and A.F. White, Mineralogical Society of America, Washington, D.C.

Deutsch, C.V.; Journel, A.G. (1998) *GSLIB Geostatistical Software Library and User's Guide* 2nd edition. Oxford University Press, New York.

Englund, E.; Sparks, A. (1991) GEO-EAS 1.2.1. *Geostatistical Environmental Assessment Software User's Guide*; EPA/600/8-91/008.

ILEPA (1998) "South Ditch Sediments" ILEPA Office of Community Relations; Springfield, IL.

Illinois Department of Natural Resources (2001) "Quality Assurance Project Plan for the DePue Wildlife Management Area. Revision 1".

Isaaks, E.H.; Srivastava, R.M. (1989) *Applied Geostatistics*. Oxford University Press, New York.

Karny, J.; Holm, T.; Kelly, W.; Wehrmann, A. (1997) "Analytical results of ground-water and surface water samples" Illinois State Water Survey internal report on the DePue diked sediment disposal area.

Locke, R. (1998) "Surveyed Locations of Sample Cores and Wells at DePue Wildlife Management Area (DWMA)" Illinois State Water Survey.

Moore, D.M. and Reynolds, R.C. (1997) *X-ray Diffraction and the Identification and Analysis of Clay Minerals*, 2nd edition, Oxford University Press, New York.

Talbott, J. and Piwoni, M. (1998) "Sample Processing and Analysis of DePue Sediments for Dr. Paul Anderson's Project" Illinois Waste Management and Research Center, Urbana, IL.

Tessier, A.; Campbell, P.G.C.; Bisson, M. (1979) "Sequential extraction procedure for the speciation of particulate trace metals" *Anal. Chem.* 51(7):844-851.

Wehrmann, A. (2001) "An assessment of metal distribution and transport in ground water beneath the diked sediment disposal area (DSDA), DePue Wildlife Management Area, Illinois" DePue Non-Time-Critical Removal Action Phase I Investigation Results, May 23, 2001.

Appendices

Appendix A. Surveyed Locations of Sample Cores and Wells at DePue Wildlife Management Area (DWMA)

Appendix B. Sample Processing and Analysis of DePue Sediments for Dr. Paul Anderson's Project

Appendix C. Raw Data for all 276 Samples.

Appendix D. Metal Speciation Extraction Data.

Appendix E. Soil Carbon Analysis Data.

Appendix A. Surveyed Locations of Sample Cores and Wells at DePue Wildlife Management Area (DWMA)

September 17, 1998

Randy Locke, ISWS, (217) 333-3866

Methods and Accuracy

Surveying of monitoring wells and sample core locations was done on September 2nd and 3rd 1998. Global Positioning System (GPS) surveying results were in geodetic coordinates with ellipsoid heights in meters. All geoid heights were calculated with the National Geodetic Survey program Geoid93. Data in metric units are expected to be accurate to +/- 0.02 meters horizontally and +/- 0.04 meters vertically. Conversions have been made to Illimap (Lambert Conformal) coordinates in feet with orthometric and ellipsoid heights in feet. Data in English units are expected to be accurate to +/- 0.07 feet horizontally and +/- 0.13 feet vertically.

The on-site reference station, DSE was used as a real-time kinematic (RTK) GPS base station. The previously calculated position for DSE (41° 18' 48.62444" N. latitude, 89° 17' 30.65420" W. longitude, and 105.711 meters ellipsoid height) was used for RTK activities. Station DSW was not used. The aluminum rod cap on DSE was approximately 1 to 2 centimeters above land surface and is subject to frost heave.

Calculated Positions

Identification flags at core locations 12-58 and 12-173 seemed to be switched (i.e., the farthest flag in cell 12 was marked as 12-58 and the second farthest was marked as 12-173). The locations given below are as they were marked in the field. In cell 5, a core hole was not found at 5-8. The surveyed position is that of the identification flag. At 3-173 and 14-173, giant ragweed and trees over 12 feet tall may have affected the accuracy of the calculated positions. Well site 10 was the only location where satellite visibility was problematic.

Core Locations (Geodetic, meters)

Core Number	Latitude (N)	Longitude (W)	Orthometric Height (m)
01-002	41 19 03.97855	89 17 39.07701	136.700
01-008	41 19 03.96750	89 17 38.98840	136.705
01-019	41 19 03.72209	89 17 38.91936	136.689
01-059	41 19 03.36036	89 17 38.27859	136.793
01-173	41 19 01.19789	89 17 38.51768	136.757
01-XAS	41 19 05.18086	89 17 36.04720	136.421
02-002	41 19 05.54624	89 17 33.64266	136.095

Core Number	Latitude (N)	Longitude (W)	Orthometric Height (m)
02-008	41 19 05.47853	89 17 33.62973	136.060
02-019	41 19 05.25368	89 17 33.45776	136.076
02-058	41 19 04.78537	89 17 33.96196	136.354
02-173	41 19 02.89711	89 17 33.78949	136.564
03-002	41 18 54.44482	89 18 15.26939	136.293
03-008	41 18 54.38917	89 18 15.22192	136.255
03-019	41 18 54.20784	89 18 14.98342	136.386
03-058	41 18 53.99472	89 18 14.22738	136.570
03-173	41 18 55.59413	89 18 12.98825	136.784
04-002	41 18 58.67908	89 18 07.57565	136.871
04-008	41 18 58.65729	89 18 07.66116	136.833
04-019	41 18 58.49782	89 18 07.91159	136.788
04-058	41 18 57.90664	89 18 07.98922	137.021
04-173	41 18 57.36893	89 18 05.64271	137.075
05-002	41 18 54.49985	89 17 56.26880	136.738
05-008	41 18 54.46159	89 17 56.20960	136.717
05-019	41 18 54.44957	89 17 55.88224	136.638
05-058	41 18 54.73550	89 17 55.15806	136.585
05-173	41 18 56.37614	89 17 56.38675	136.432
06-002	41 18 58.55941	89 17 46.79660	136.614
06-008	41 18 58.53999	89 17 46.88815	136.623
06-019	41 18 58.41719	89 17 47.16998	136.457
06-058	41 18 58.11508	89 17 47.85990	136.421
06-173	41 18 56.93581	89 17 45.97069	136.948
07-002	41 18 57.01430	89 17 37.46722	137.147
07-008	41 18 57.02406	89 17 37.55852	137.081
07-019	41 18 56.93941	89 17 37.87887	137.164
07-058	41 18 56.50143	89 17 38.48857	136.980
07-173	41 18 56.62806	89 17 41.14247	136.852
08-002	41 18 54.81614	89 17 32.78227	136.881
08-008	41 18 54.83704	89 17 32.87550	136.894
08-019	41 18 54.93854	89 17 33.16759	136.912
08-058	41 18 55.24549	89 17 33.90269	136.997

Core Number	Latitude (N)	Longitude (W)	Orthometric Height (m)
08-173	41 18 56.98781	89 17 33.22013	136.667
09-002	41 18 50.74131	89 18 15.30958	136.677
09-008	41 18 50.80656	89 18 15.32300	136.664
09-019	41 18 51.03763	89 18 15.17821	136.608
09-058	41 18 51.64612	89 18 15.14954	136.407
09-173	41 18 51.33345	89 18 12.69029	136.855
10-002	41 18 50.02617	89 18 02.55429	136.850
10-008	41 18 49.95228	89 18 02.53928	136.870
10-019	41 18 49.70651	89 18 02.56254	136.801
10-058	41 18 49.26273	89 18 03.09426	136.835
10-173	41 18 50.36788	89 18 05.00541	136.567
11-002	41 18 49.08351	89 17 53.77742	136.640
11-008	41 18 49.11383	89 17 53.85022	136.650
11-019	41 18 49.21294	89 17 54.20632	136.674
11-058	41 18 48.95653	89 17 54.94618	136.684
11-173	41 18 50.67089	89 17 56.31187	136.669
12-002	41 18 51.11384	89 17 48.18242	136.968
12-008	41 18 51.09098	89 17 48.26255	136.962
12-019	41 18 51.26752	89 17 48.49362	136.973
12-058	41 18 51.91016	89 17 51.11136	136.885
12-173	41 18 50.87699	89 17 49.10601	136.899
13-002	41 18 49.45939	89 17 40.63670	136.194
13-008	41 18 49.51372	89 17 40.67112	136.196
13-019	41 18 49.75347	89 17 40.75620	136.426
13-058	41 18 49.85991	89 17 41.66143	136.611
13-173	41 18 51.81139	89 17 41.72240	136.638
14-002	41 18 49.44422	89 17 31.70647	136.409
14-008	41 18 49.48717	89 17 31.78315	136.461
14-019	41 18 49.74273	89 17 31.77242	136.518
14-058	41 18 50.28162	89 17 31.41249	136.321
14-173	41 18 52.03154	89 17 32.87633	137.132

Core Locations (Illimap, feet)

Core Number	Northing (ft)	Easting (ft)	Orthometric Height (ft)
01-002	10027224.730	9896000.973	448.491
01-008	10027247.696	9895997.692	448.507
01-019	10027264.100	9895915.671	448.455
01-059	10027424.862	9895797.561	448.796
01-173	10027365.806	9895082.338	448.678
01-XAS	10027979.324	9896397.954	447.575
02-002	10028576.436	9896522.626	446.506
02-008	10028579.717	9896499.661	446.391
02-019	10028622.368	9896424.201	446.444
02-058	10028497.696	9896270.002	447.356
02-173	10028543.628	9895646.642	448.045
03-002	10018212.263	9892828.401	447.156
03-008	10018225.386	9892811.996	447.031
03-019	10018284.441	9892749.660	447.461
03-058	10018474.730	9892680.763	448.064
03-173	10018779.848	9893208.978	448.766
04-002	10020128.273	9894232.600	449.052
04-008	10020105.308	9894226.038	448.927
04-019	10020042.972	9894173.545	448.780
04-058	10020026.567	9893976.695	449.544
04-173	10020610.557	9893799.529	449.721
05-002	10022946.515	9892857.928	448.615
05-008	10022962.919	9892844.805	448.547
05-019	10023044.940	9892841.524	448.287
05-058	10023225.386	9892936.668	448.114
05-173	10022916.987	9893478.007	447.612
06-002	10025305.439	9894206.353	448.209
06-008	10025282.473	9894199.792	448.238
06-019	10025213.575	9894157.141	447.694
06-058	10025039.691	9894058.716	447.575
06-173	10025512.132	9893668.296	449.304
07-002	10027631.554	9893697.823	449.957
07-008	10027608.589	9893701.104	449.741

Core Number	Northing (ft)	Easting (ft)	Orthometric Height (ft)
07-019	10027529.848	9893674.857	450.013
07-058	10027375.649	9893530.500	449.409
07-173	10026716.200	9893569.870	448.990
08-002	10028799.534	9892976.038	449.085
08-008	10028776.568	9892982.600	449.127
08-019	10028704.389	9893015.408	449.186
08-058	10028520.662	9893117.114	449.465
08-173	10028687.985	9893694.542	448.383
09-002	10018205.701	9891604.647	448.415
09-008	10018202.420	9891627.613	448.373
09-019	10018238.510	9891703.072	448.189
09-058	10018245.071	9891903.204	447.530
09-173	10018858.588	9891801.498	448.999
10-002	10021384.835	9891374.988	448.983
10-008	10021388.116	9891352.023	449.049
10-019	10021381.554	9891270.002	448.822
10-058	10021250.321	9891122.364	448.934
10-173	10020774.599	9891486.537	448.054
11-002	10023573.155	9891069.870	448.294
11-008	10023553.470	9891079.713	448.327
11-019	10023464.888	9891112.521	448.406
11-058	10023281.161	9891027.219	448.438
11-173	10022939.953	9891591.524	448.389
12-002	10024964.232	9891742.443	449.370
12-008	10024944.547	9891735.881	449.350
12-019	10024888.772	9891794.936	449.386
12-058	10024235.885	9892004.910	449.098
12-173	10024734.573	9891663.702	449.144
13-002	10026847.434	9891201.104	446.831
13-008	10026837.591	9891217.508	446.837
13-019	10026817.906	9891296.248	447.592
13-058	10026591.528	9891332.338	448.199
13-173	10026575.124	9891978.663	448.287

Core Number	Northing (ft)	Easting (ft)	Orthometric Height (ft)
14-002	10029071.843	9891201.104	447.536
14-008	10029052.158	9891214.227	447.707
14-019	10029055.439	9891299.529	447.894
14-058	10029144.022	9891476.694	447.247
14-173	10028779.848	9892054.122	449.908

Well Locations (Geodetic, meters)

Well Number	Latitude (N)	Longitude (W)	Measuring Point Height (m)
1-15P	41 18 44.68292	89 17 29.84355	137.932
2-15P	41 18 41.48419	89 17 47.77574	137.888
3-15P	41 18 35.44181	89 18 03.95864	137.940
4-15P	41 18 31.54908	89 18 15.13878	138.277
5-10P	41 19 00.99796	89 17 30.23961	136.846
6-10P	41 18 48.32193	89 17 30.39486	137.123
7-10P	41 18 47.71926	89 17 51.99835	137.393
8-10P	41 18 47.70948	89 18 07.75588	137.117
9-10P	41 18 59.11633	89 18 16.08751	136.134
10-10P	41 18 57.65130	89 18 02.31126	136.512
11-10P	41 18 59.14704	89 17 42.07278	136.709
14-15P	41 18 58.48098	89 17 46.55089	137.246
18-15P	41 19 02.31073	89 17 12.50117	136.932

Well Locations (Illimap, feet)

Well Number	Northing (ft)	Easting (ft)	Measuring Point Height (ft)
1-15P	10029541.003	9889629.582	452.533
2-15P	10025072.499	9888560.028	452.388
3-15P	10021046.909	9886555.434	452.559
4-15P	10018261.475	9885262.784	453.665
5-10P	10029429.455	9895020.002	448.970
6-10P	10029399.927	9890830.369	449.879
7-10P	10024016.069	9890620.395	450.764
8-10P	10020088.903	9890607.272	449.859
9-10P	10018005.570	9894373.676	446.634
10-10P	10021440.609	9893894.674	447.874
11-10P	10026483.260	9894403.204	448.520
14-15P	10025367.775	9894180.107	450.282

18-15P	10033848.746	9895462.915	449.252

Appendix B. Sample Processing and Analysis of DePue Sediments for Dr. Paul Anderson's Project

by

Jonathan Talbott, PhD

and

Marvin Piwoni, PhD

Illinois Waste Management and Research Center

with contributions from Luann Wiedenmann, Paul Fish and John Scott

Background

This report of sample processing and analysis of Dr. Paul Anderson's samples is a revised version of an overall report entitled "The Determination of Metals in Sediments of the DePue Wildlife Management Area". It is a revision of the overall report as Dr. Paul Anderson's project focussed on just four metals (zinc, copper, cadmium and lead) and samples were sectioned and characterized differently. A full report on metals analyses conducted by the Waste Management and Research Center on all DePue sediments will be made available in the near future.

Sectioning of Cores

Cores were received at the Waste Management and Research Center under custody of either Dr. Jonathan Talbott or Monte Wilcoxon upon return from the sampling trip. Cores were initially stored at room temperature. Upon observation of mold growth in a few samples, cores were moved to the walk-in refrigerator were they remained until characterization and sectioning of cores occurred.

Each core, approximately four feet depending upon recovery, was briefly described and characterized prior to analysis. Copies of all core descriptions were attached to the first report as these were needed to explain how cores were segmented and each segment of core was analyzed. For the most part, cores were sectioned into 30 centimeter lengths and each section was dried, ground microwave digested by method 3050 and analyzed. However, there were a few instances were smaller sections were obtained as unique sediment properties warranted (sand lenses, etc). Prior data of the DePue Wildlife Management Area indicated that depth profiles exist for most metals.

Sample Preparation - Drying and Grinding

The drying and grinding procedure is fully detailed elsewhere [1].

Sections of cores were subsampled for drying at a minimum of 4 locations to obtain subsamples representative of the whole section. Approximately 30 grams of each section, accurately weighed, were taken for drying. Subsamples were dried to constant weight in ceramic evaporating dishes at 105 ^{o}C such that percent moistures could be determined. Dried sediments

were then ground and homogenized to a fine face powder (particle diameter < 10 microns) with a ceramic ram "puck" in a sealed vessel in a Gy-Ro Mill for 8 minutes. Powdered samples were then transferred to polypropylene bottles and stored in desiccators until they could be acid digested into solution.

Sample Digestion

The microwave acid digestion procedure used on the DePue sediments is fully described elsewhere [2.] This procedure is essentially the Waste Management and Research Center's implementation of the USEPA's SW-846 Method 3051 [3]. The microwave procedure is as follows. Samples were processed in analytical batches of a maximum of 24 samples. An analytical batch consisted of up to two microwave carousels of 12 samples each with both carousels processed within the same day. Each batch contained it's own complete set of batch QC samples including 2 digested reagent blanks, a duplicate sample, a minimum of one matrix spike sample, and a laboratory control standard (NIST standard reference material 2710). When 24 samples were processed, three matrix spikes at different concentration levels were prepared in an attempt to assure that at least one matrix spike would be close to the concentration range observed within the selected sample.

One half grams of each dried and ground sediment sample, accurately weighed, were transferred to CEM Advanced Composite Vessels (ACVs). Five milliliters of DI water and 10 milliliters of concentrated nitric acid, trace metals grade, were added to all samples, blanks, and standards. Vessels were then capped and heated in a CEM Model 205 microwave under pressure control for 1 minute at 50% power then at 11 minutes at 80% power to dissolve the analytes of interest into solution. Upon completion of the digestion, all samples, blanks and standards were filtered through Whatman #40 filters to remove undigested residues (mostly insolubilized silicates). Filtrates were then taken up to constant volume in 100 mL volumetric flasks and transferred to precleaned Nalgene® bottles for storage until analyses could be performed.

Sample Analyses

Digestates were analyzed by Inductively Coupled Plasma Mass Spectrometry (ICP-MS)[4]. Although the ICP-MS standard operating procedure for the DePue project is fully described elsewhere [5], a brief summary is provided here.

Experimental

Reagents and Solutions

Multi-element standards (Spex Industries, Edison, NJ) were used for preparation of ICP-MS calibration standards. Independent calibration check standards solutions were either separate lots of the calibration standards or were from Sigma Chemical Co. (St. Louis, MO). All internal standards were single element from Spex Industries. All working solutions were 2 % wt/vol HNO_3 prepared from Optima® Grade concentrated nitric acid (Pittsburgh, PA). ASTM Type I water (resistivity > 18 MΩ, Labconoco, Kansas City, MO) was used throughout.

Instrumentation

A Perkin-Elmer Sciex ELAN 5000 (Perkin-Elmer Corporation, Norwalk, CT) ICP-MS was used for measurements. Experimental conditions of the instrument and of operating conditions are summarized below.

Table 1: Operating conditions for the ELAN 5000

Plasma	
Rf power/Watts	1015
Gas flow	
Plasma/ L min^{-1}	12.5
Nebulizer/L min^{-1}	0.91
Auxiliary/L min^{-1}	0.8
Ion sampling-	
Sampler Cone	Nickel, 0.89 mm orifice
Skimmer Cone	Nickel, 1.1 mm orifice
Vacuum-	
Analyzer stage/torr	1.1 X 10^{-5}
Quantitation Parameters	
Dwell Time	20 ms
Sweeps/Reading	40
Replicates	3
Points/Spectral Peak	3
Scanning Mode	Peak Hop
Resolution	Normal
Isotopes monitored	^{63}Cu, ^{66}Zn, ^{111}Cd, and ^{208}Pb
Internal Standards	^{45}Sc (for Cu and Zn), ^{103}Rh (for Cd) and 232Th (for Pb)

Each element of interest was calibrated at the mass (m/z) of a specific isotope identified in the Table above. The instrument was calibrated for each element at a minimum of 6 points (not including the blank) over a concentration range from 1 to 100 ng/mL. Internal standards, at relatively high concentrations, were added in-line to all standards, samples, and blanks through the use of a mixing T. Internal standards not only minimize instrument drift but also correct for some sample matrix effects such as viscosity differences. Acceptance criteria were established for both the linearity of the calibration curves and recovery of the internal standards in all samples.

Independent calibration check standards, at both low and high concentrations within the calibration curve, were analyzed before and after every 10 samples, of portion there of, throughout the analysis run to ensure that the instrument remained in calibration during the run.

For sample results to be acceptable, results of independent calibration check standards must have met specific acceptance criteria (generally ±10% of true values) identified within the SOP[5].

Samples were analyzed at minimum 10-fold dilutions for zinc, copper and lead and at minimum 4-fold dilutions, if necessary, for cadmium. Samples with overrange results were diluted until results within the calibration range were obtained. Analytical spikes were performed during an analysis run, when it was determined that matrix spikes were not spiked at a concentration close to that of the sample.

After analysis, data files were transferred to spreadsheet workstations were sample data could be processed. All batch quality control parameters were evaluated relative to their own specific acceptance criteria for acceptance of the sample data. Failure of batch quality control parameters meant that samples would be required to be reprepared for analytes with unacceptable QC. Results are reported on forms specific for the DePue project in accordance to the SOP[5]. Sample results are reported on a dry weight basis and have been corrected for all dilutions and sample preparation.

References

1. Illinois Waste Management and Research Center, Standard Operating Procedure for Solid Sediments Preparation: Drying (% Moisture Determination) and Grinding, 1/6/98.
2. Illinois Waste Management and Research Center, Standard Operating Procedure for Sample Digestion of DePue Sediments, 1/7/98.
3. U. S. Environmental Protection Agency (USEPA), Method 3051, "Microwave Assisted Acid Digestion of Sediments, Sludges, Soils, and Oils" in *Test Methods for Evaluating Solid Waste, Physical/Chemical Methods, SW-846*, Office of Solid Waste and Emergency Response, Washington, D.C., 20460, December 1996.
4. U. S. Environmental Protection Agency (USEPA), Method 6020, "Inductively Coupled Plasma – Mass Spectrometry" in *Test Methods for Evaluating Solid Waste, Physical/Chemical Methods, SW-846*, Office of Solid Waste and Emergency Response, Washington, D.C., 20460, November 1992.
5. Illinois Waste Management and Research Center, Laboratory Method for ICP-MS Analysis of Metals in Sediments in the DePue Project, 2/3/98.

Appendix C. Raw Data for all 276 Samples.

This table includes sample identification, average depth (cm), metal concentrations (mg/kg), and solids content (%) for all 276 samples.

Core Identification	Average Depth	Cd	Cu	Pb	Zn	Solids
1-2 (0-30 cm)	15	86	149	534	5240	73.9
1-2 (30-60 cm)	45	53	83	271	3330	74.3
1-2 (60-90 cm)	75	58	84	215	3030	71.3
1-2 (90-118 cm)	104	15	68	92	600	73.2
1-8 (0-30 cm)	15	75	107	363	4420	73.9
1-8 (30-60 cm)	45	66	88	261	3700	71.8
1-8 (60-96 cm)	78	20	72	114	944	73.2
1-19 (0-30 cm)	15	62	95	240	3490	74.4
1-19 (30-60 cm)	45	77	99	304	4280	71.8
1-58 (0-30 cm)	15	69	97	287	3610	72.5
1-58 (30-53 cm)	42	83	100	298	4480	70.4
1-58 (53-85 cm)	69	12	67	94	568	73.6
1-173 (0-30 cm)	15	91	133	439	5490	70.7
1-173 (30-65 cm)	48	72	93	266	4390	71
1-173 (65-100 cm)	83	15	70	99	697	73.2
2-2 (0-30 cm)	15	54	86	241	3470	71
2-2 (30-60 cm)	45	103	97	307	4960	64.4
2-2 (60-95 cm)	78	57	78	240	3240	62.4
2-8 (0-30 cm)	15	42	79	239	3430	70.4
2-8 (30 60 cm)	45	68	81	258	3930	67.3
2-8 (60-90 cm)	75	59	81	251	3760	63.5
2-8 (90-103 cm)	97	61	78	228	3670	60.8
2-19 (0-30 cm)	15	75	111	422	5200	69.5
2-19 (30- 60 cm)	45	65	89	302	4090	67.4
2-19 (60-98 cm)	79	53	84	239	3310	63.3
2-58 (0-5 cm)	3	49	86	218	3010	71.9
2-58 (5-16 cm)	11	31	63	129	2190	70.4
2-58 (16-81 cm)	49	39	78	205	2790	69.1
2-173 (0-30 cm)	15	79	112	314	5060	70
2-173 (30-60 cm)	45	57	82	224	3270	71.8

2-173 (60-90 cm)	75	40	100	165	1860	70.0
3-2 (0-30cm)	15	64	92	159	3930	70.9
3-2 (30-60cm)	45	55	82	156	3020	67.4
3-2 (60-90cm)	75	43	76	162	2890	66.4
3-2 (90-104cm)	97	88	157	422	7300	62.3
3-8 (0-30cm)	15	59	92	163	3870	68.8
3-8 (30-60cm)	45	52	86	152	3290	67.6
3-8 (60-90cm)	75	44	91	166	3240	65.6
3-8 (90-118cm)	104	87	142	363	5450	62
3-19 (0-30cm)	15	53	89	165	3660	73.5
3-19 (30-60cm)	45	66	99	199	4050	68.1
3-19 (60-90cm)	75	56	82	158	3010	68.2
3-19 (90-114cm)	102	109	195	444	7110	65.5
3-58 (0-30cm)	15	50	113	174	4130	73.7
3-58 (30-60cm)	45	59	93	174	3640	70.8
3-58 (60-90cm)	75	55	88	171	3460	68.2
3-58 (90-116cm)	103	68	111	284	3960	67.1
3-58R (0-30cm)	15	63	122	201	4360	72.7
3-58R (30-60cm)	45	75	95	203	4460	68.3
3-58R (60-93cm)	76.5	54	117	284	3940	65.7
3-173 "willows" (0-30 cm)	15	51	97	177	3610	70.3
3-173 "willows" (30-60 cm)	45	66	150	394	4460	66.1
3-173 (0-30 cm)	15	55	102	180	3740	72.3
3-173 (30-65 cm)		58	111	252	3870	68.1
4-2 (0-30cm)	15	68	110	209	4420	72.5
4-2 (30-46cm)	38	36	69	125	2300	72
4-2 (46-50cm)	48	7	9	12	460	93.6
4-2 (50-77cm)	63.5	13	26	32	1290	80.5
4-2 (77-82cm)	79.5	24	54	77	1840	66.9
4-8 (0-30cm)	15	65	94	188	4230	69.8
4-8 (30-47cm)	38.5	31	75	132	2090	69.7
4-8 (47-80cm)	63.5	13	26	47	1350	79.4
4-8 (80-88cm)	84	23	55	81	2030	69.7
4-19 (0-30cm)	15	51	85	174	3440	69.3
4-19 (30-49.5cm)	39.5	34	90	129	2340	67.9

4-19 (49.5-65cm)	57.25	29	54	105	2480	75.1
4-19 (65-91cm)	78	27	67	91	2660	69.2
4-58 (0-30cm)	15	69	96	206	4300	70.8
4-58 (30-60cm)	45	46	77	157	3090	69.6
4-58 (60-78.5cm)	69.25	43	81	175	2870	66.8
4-58 (78.5-106.5cm)	92.5	30	52	82	2350	71.5
4-58R (0-30cm)	15	54	85	165	3610	73.9
4-58R (30-69.5cm)	49.75	55	84	180	3540	68.8
4-58R (69.5-96cm)	82.75	35	64	109	2920	69.3
4-173 (0-30cm)	15	43	65	137	2770	76.6
4-173 (30-63cm)	46.5	65	91	192	4500	70.8
4-173 (63-94cm)	78.5	18	31	57	1560	78.2
4-173 (94-100cm)	97	22	51	78	1950	68.2
5-2 (0-30cm)	15	96	165	507	5470	71.2
5-2 (30-60cm)	45	61	85	263	3680	70
5-2 (60-90cm)	75	32	69	142	1900	73.5
5-2 (90-103.5cm)	96.75	16	86	108	649	74.9
5-8 (0-30cm)	15	112	243	794	6800	71.7
5-8 (30-60cm)	45	56	84	258	3420	71.2
5-8 (60-90cm)	75	51	74	203	3170	71.6
5-8 (90-117cm)	103.5	21	93	133	761	74.2
5-19 (0-30cm)	15	87	115	295	4640	71.4
5-19 (30-60cm)	45	51	78	227	3210	71
5-19 (60-90cm)	75	51	65	175	2640	71.5
5-19 (90-120cm)	105	24	87	139	1150	72.2
5-19R (0-30cm)	15	83	115	246	4710	72.2
5-19R (30-52cm)	41	63	87	250	3600	70.5
5-19R (52-85cm)	68.5	45	69	177	2590	70.4
5-19R (85-104cm)	94.5	14	76	104	573	73.8
5-58 (0-30cm)	15	82	144	385	5140	71.4
5-58 (30-60cm)	45	65	91	272	3760	69.8
5-58 (60-90 cm)	75	56	91	218	3390	70.4
5-58 (90-117cm)	103.5	15	102	111	631	74.6
5-173 (0-30 cm)	15	122	312	903	7140	71.8
5-173 (30-60 cm)	45	51	81	204	3110	72.6

5-173 (60-90 cm)	75	35	58	152	2080	74.8
5-173 (90-118 cm)	104	25	44	116	1540	77.3
6-2 (0-30 cm)	15	108	165	472	5850	69.4
6-2 (30-60 cm)	45	73	107	251	4360	68.7
6-2 (60-90 cm)	75	47	100	192	2550	71.4
6-2 (90-115 cm)	102.5	15	98	97	585	72.0
6-8 (0-30 cm)	15	158	385	1580	9400	68.6
6-8 (30-60 cm)	45	100	219	840	6130	68.2
6-8 (60-90 cm)	75	74	137	382	4620	68.0
6-8 (90-117)	103.5	20	100	120	785	74.1
6-19 (0-30 cm)	15	147	328	1210	9590	70.1
6-19 (30-60 cm)	45	56	98	226	3320	71.3
6-19 (60-90 cm)	75	56	86	221	3100	69.1
6-19 (90-116 cm)	103	53	93	176	2340	69.3
6-58 (0-30 cm)	15	252	769	2650	15200	68.8
6-58 (30-60 cm)	45	149	494	1770	8780	70.2
6-58 (60-90 cm)	75	52	71	174	2980	69.9
6-58 (90-109 cm)	99.5	12	66	105	831	71.6
6-173 (0-30 cm)	15	112	227	629	6700	73.1
6-173 (30-60 cm)	45	69	103	292	3840	70.0
6-173 (60-90 cm)	75	19	80	108	899	73.8
6-173 (90-116.5 cm)	103.25	15	85	98	557	74.2
6-173R (0-30 cm)	15	69	117	258	4380	72.9
6-173R (30-60 cm)	45	76	110	320	4240	70.5
6-173R (60-90 cm)	75	14	81	103	588	74.3
6-173R (90-113 cm)	101.5	16	94	108	627	74.8
7-2 (0-30 cm)	15	52	78	197	3300	71.9
7-2 (30-60 cm)	45	28	66	136	1730	72.7
7-2 (60-84 cm)	72	11	63	101	510	73.3
7-8 (0-30 cm)	15	66	101	283	4600	73.3
7-8 (30-51 cm)	40.5	73	97	280	4570	71.8
7-8 (51-81 cm)	66	8	55	78	410	74.8
7-8 (81-98 cm)	89.5	18	85	123	730	74.3
7-19 (0-34 cm)	17	67	90	265	4110	72.0
7-19 (34-73 cm)	53.5	12	68	100	505	74.6

7-58 (0-30 cm)	15	65	91	274	4380	74.7
7-58 (30-39 cm)	34.5	74	100	286	4380	68.3
7-58 (39-69 cm)	54	7	60	81	380	77.0
7-58 (69-94 cm)	81.5	13	78	94	540	74.5
7-173 (0-36 cm)	18	71	96	286	4380	72.9
7-173 (36-74 cm)	55	18	79	104	980	73.9
8-2 (0-30 cm)	15	55	91	240	3530	74.9
8-2 (30-60 cm)	45	25	67	146	1570	76.8
8-2 (60-90 cm)	75	14	87	102	636	78.9
8-2 (90-112 cm)	101	5	76	93	470	76.7
8-8 (0-30 cm)	15	75	109	293	4700	73.9
8-8 (30-60 cm)	45	22	71	135	1520	76.5
8-8 (60-90 cm)	75	14	87	101	633	78.0
8-8 (90-114 cm)	102	5	70	85	455	74.4
8-19 (0-30 cm)	15	56	93	219	3630	74.0
8-19 (30-60 cm)	45	24	69	140	1470	76.9
8-19 (60-90 cm)	75	17	97	114	686	79.1
8-19 (90-102 cm)	96	6	71	91	430	76.0
8-58R (30-60 cm)	45	19	72	99	1090	76.2
8-58R (60-90 cm)	75	13	75	95	552	78.0
8-58R (90-104 cm)	97	9	79	95	451	75.6
8-58R (0-30 cm)	15	58	102	247	3730	72.3
8-58R (0-30 cm)	15	55	92	225	3310	73.8
8-58R (30-48.5 cm)	39.25	53	86	184	3060	73.9
8-58R (48.5-70.5 cm)	59.5	8	74	75	345	77.4
8-58R (70.5-113 cm)	91.75	14	86	97	536	76.7
8-173 (0-30 cm)	15	32	67	172	1960	75.6
8-173 (30-60 cm)	45	13	77	103	554	78.7
8-173 (60-90 cm)	75	13	82	93	514	76.7
8-173 (90-104 cm)	97	3	61	84	449	74.8
9-2 (0-30 cm)	15	32	110	135	3240	73.7
9-2 (30-60 cm)	45	42	86	176	2850	71.3
9-2 (60-85 cm)	72.5	59	116	314	3790	71.7
9-8 (0-30 cm)	15	49	99	169	3660	73.5
9-8 (30-60 cm)	45	44	81	176	3000	72.3

9-8 (60-90 cm)	75	38	73	153	2640	72.3
9-19 (0-30 cm)	15	42	101	145	3460	73.4
9-19 (30-60 cm)	45	45	86	174	2810	71.6
9-19 (60-90 cm)	75	57	115	305	3990	70.8
9-19 (90-101 cm)	95.5	60	144	336	3640	69.4
9-58 (0-30 cm)	15	58	94	200	3660	69.9
9-58 (30-60 cm)	45	51	116	284	3490	67.7
9-58 (60-71 cm)	65.5	55	158	176	4840	63.2
9-173 (0-33 cm)	16.5	25	84	148	1480	72.0
9-173 (33-63 cm)	48	52	96	146	3920	72.5
10-2 (0-30 cm)	15	54	107	182	3520	73.3
10-2 (30-60 cm)	45	53	94	182	3350	72.2
10-2 (60-90 cm)	75	51	108	229	3270	70.8
10-2 (90-108 cm)	99	13	86	101	565	75.6
10-8 (0-30 cm)	15	45	110	179	3530	72.2
10-8 (60-90 cm)	75	63	102	228	3900	70.1
10-8 (30-60 cm)	45	48	93	170	3120	72
10-8 (90-122 cm)	106	16	126	120	852	75.3
10-8R (0-30 cm)	15	57	124	196	3980	71.7
10-8R (30-60 cm)	45	39	84	160	2560	71.9
10-8R (60-90 cm)	75	14	114	105	569	75.4
10-8R (90-102 cm)	96	36	129	179	2240	72.8
10-19 (0-30 cm)	15	47	125	177	3210	70.6
10-19 (30-60 cm)	45	41	89	162	2750	70.6
10-19 (60-90 cm)	75	58	135	223	3250	71
10-19 (90-111 cm)	100.5	10	82	90	486	74
10-58 (0-30 cm)	15	31	120	124	2440	73
10-58 (30-60 cm)	45	55	117	180	3830	72.3
10-58 (60-90 cm)	75	48	95	180	3220	71.8
10-58 (90-104 cm)	97	44	97	194	2590	72.4
10-173 (0-30 cm)	15	67	129	218	4460	72.9
10-173 (30-60 cm)	45	52	89	174	3230	70.7
10-173 (60-90 cm)	75	35	71	153	2430	69.4
10-173 (90-105 cm)	97.5	90	110	283	5520	67.8
11-2 (0-30 cm)	15	58	105	188	3450	74.2

11-2 (30-60 cm)	45	54	88	188	3480	71.9
11-2 (60-77 cm)	68.5	40	78	172	2520	85.4
11-8 (0-30 cm)	15	55	99	188	3600	74.0
11-8 (30-60 cm)	45	46	85	176	3190	70.0
11-8 (60-71 cm)	65.5	23	72	136	1820	70.9
11-19 (0-30 cm)	15	65	96	208	3970	73.6
11-19 (30-60 cm)	45	44	82	180	2740	71.5
11-19 (60-82 cm)	71	6	69	92	461	75.0
11-58 (0-30 cm)	15	46	116	158	3675	74.5
11-58 (30-61 cm)	45.5	43	79	163	2450	72.3
11-173 (0-30 cm)	15	71	116	257	4182	71.9
11-173 (30-60 cm)	45	50	90	183	2880	71.7
11-173 (60-90 cm)	75	15	72	107	827	74.0
11-173 (90-99 cm)	94.5	3	76	99	457	73.4
12-2 (0-30 cm)	15	64	94	191	4030	72.5
12-2 (30-60 cm)	45	19	70	97	1170	75.9
12-2 (60-94 cm)	77	12	73	97	581	76
12-8 (0-30 cm)	15	67	108	210	4330	74.6
12-8 (30-60 cm)	45	40	78	141	2550	72.8
12-8 (60-90 cm)	75	9	63	85	432	77.2
12-8 (90-101 cm)	95.5	15	83	97	590	76
12-19 (0-30 cm)	15	76	104	223	4830	71.9
12-19 (30-55 cm)	42.5	49	84	174	3110	77.6
12-19 (55-85 cm)	70	10	71	85	520	77.6
12-19 (85-114)	99.5	16	86	106	684	75.9
12-58 (0-30 cm)	15	61	113	212	3748	75.2
12-58 (30-60 cm)	45	34	73	147	1948	75.6
12-58 (60-89 cm)	74.5	11	74	95	433	77.4
12-173 (0-30 cm)	15	70	92	226	3950	72.8
12-173 (30-60 cm)	45	16	69	95	861	77.4
12-173 (60-90 cm)	75	11	70	87	463	77
12-173 (90-100 cm)	95	13	77	92	507	77
13-2 (0-30 cm)	15	44	76	150	2660	71.9
13-2 (30-60 cm)	45	12	76	91	569	75
13-2 (60-90 cm)	75	6.4	85	105	522	73.2

13-2 (90-113 cm)	102	2.5	58	87	406	73
13-2-R (0-30 cm)	15	37	76	148	1908	73.3
13-2-R (30-60 cm)	45	9	80	101	443	75.0
13-2-R (60-90 cm)	75	3	69	102	429	72.5
13-2-R (90-100 cm)	95	1	20	25	171	74.8
13-8 (0-30 cm)	15	41	79	132	2010	72.2
13-8 (30-60 cm)	45	15	84	102	628	76.3
13-8 (60-90 cm)	75	5	77	101	488	72.8
13-8 (90-116cm)	103	2	35	42	292	73.0
13-19 (0-30 cm)	15	61	88	181	3630	73.7
13-19 (30-60 cm)	45	40	87	148	2300	74.6
13-19 (60-90 cm)	75	12	78	90	540	76.3
13-19 (90-115 cm)	102.5	5	90	117	572	73.5
13-58 (0-30 cm)	15	38	72	164	2301	74.8
13-58 (30-60 cm)	45	35	75	160	2049	73.9
13-58 60-88 cm)	74	7	75	109	473	75.2
13-173 (0-30 cm)	15	43	75	166	2433	73.1
13-173 (30-60 cm)	45	37	81	165	2370	73.3
13-173 (60-90 cm)	75	14	86	107	537	82.1
13-173 (90-100 cm)	95	4	87	124	609	72.5
14-2 (0-30 cm)	15	45	76	194	2830	75.0
14-2 (30-60 cm)	45	37	62	176	2310	72.3
14-2 (60-70 cm)	65	1	16	16	112	77.4
14-8 (0-30 cm)	15	49	84	217	3100	74.3
14-8 (30-60 cm)	45	35	61	180	2220	73.4
14-8 (60-93 cm)	76.5	12	30	75	763	76.1
14-19 (0-30 cm)	15	50	85	241	2830	75.7
14-19 (30-60 cm)	45	44	69	205	2460	74.7
14-19 (60-90 cm)	75	4	22	34	267	76.8
14-58 (0-30 cm)	15	58	92	260	3440	74.2
14-58 (30-60 cm)	45	48	79	191	2520	70.6
14-58 (60-68 cm)	64	5	29	39	338	76.1
14-173 (0-30 cm)	15	49	78	178	2680	79.2
14-173 (30-60 cm)	45	33	76	181	1910	75.1
14-173 (60-90 cm)	75	13	69	104	570	79.3

14-173 (90-118 cm)	104	4	65	108	470	76.2

Appendix D. Metal Speciation Extraction Data.

This table summarizes mean (and standard deviation) for each fraction. Values are expressed as mg/kg measured from 12 samples.

Fraction	Cd	Cu	Pb	Zn
Exchangeable	54.9 (4.2)	0.6 (0.08)	0.3 (0.1)	3.8 (1.6)
Carbonate	22.5 (2.5)	3.8 (1.4)	10.6 (3.7)	27.4 (2.9)
Fe & Mn Oxide	19.6 (2.6)	13.2 (2.2)	48.7 (1.6)	53.4 (3.1)
Organic Matter	2.1 (0.3)	42.3 (5.3)	18.8 (1.7)	8.5 (0.7)
Residual	0.8 (0.1)	40.2 (6.3)	21.6 (4.4)	6.9 (1.0)

Appendix E. Soil Carbon Analysis Data.

Identification	Description	Total Carbon, %	TIC, %	TOC %
3-2 (0-30 cm)	Depth Profile Series, Black massive blocky throughout series	3.50	0.66	2.84
3-2 (30-60 cm)	Depth Profile	3.72	0.58	3.15
3-2 (60-90 cm)	Depth Profile	3.83	0.60	3.23
3-2 (90-104 cm)	Depth Profile - Clay	4.26	0.75	3.51
6-58 (0-30 cm)	Depth Profile Series, Blocky, massive throughout, orange in cracks	5.41	0.61	4.80
6-58 (30-60 cm)	Depth Profile	4.93	0.66	4.27
6-58 (60-90 cm)	Depth Profile	2.99	0.74	2.25
6-58 (90-108 cm)	Depth Profile, black clay	3.38	0.65	2.73
4-19 (49.5-65 cm)	Sandy Laminae	2.59	1.15	1.44
4-58 (60-78.5 cm)	Fine Sand lens	3.87	0.57	3.30
2-2 (60-95 cm)	Very wet, won't break apart	3.53	0.88	2.65
2-58 0-5cm	Top Soil	4.36	0.65	3.71


ILLINOIS
DEPARTMENT OF
NATURAL
RESOURCES